의학박사 학위논문

Analysis of Retinal Proteome in Oxygen-induced Retinopathy

산소유발망막병증 모델의
망막 단백체 분석

2013년 2월

서울대학교 대학원
의학과 안과학 전공
김 상 진

Analysis of Retinal Proteome in Oxygen-induced Retinopathy

지도교수 유 형 곤

이 논문을 의학박사 학위논문으로 제출함

2012년 10월

서울대학교 대학원

의학과 안과학 전공

김 상 진

김상진의 박사 학위논문을 인준함

2012년 12월

위 원 장 위 원 량 (인)

부위원장 유 형 곤 (인)

위 원 김 영 수 (인)

위 원 이 정 렬 (인)

위 원 윤 영 희 (인)

Analysis of Retinal Proteome in Oxygen-induced Retinopathy

by

Sang Jin Kim

A Thesis Submitted to the Department of Medicine in Partial Fulfilment of the Requirements for the Degree of Doctor of Philosophy in Medicine (Ophthalmology) at the Seoul National University College of Medicine

December 2012

Approved by thesis committee:

Professor	Won Ryang Wee	Chairman
Professor	Hyeong Gon Yu	Vice Chairman
Professor	Youngsoo Kim	
Professor	Jeong Ryul Lee	
Professor	Young Hee Yoon	

학위논문 원문제공 서비스에 대한 동의서

본인의 학위논문에 대하여 서울대학교가 아래와 같이 학위논문 저작물을 제공하는 것에 동의합니다.

1. 동의사항
   ① 본인의 논문을 보존이나 인터넷 등을 통한 온라인 서비스 목적으로 복제할 경우 저작물의 내용을 변경하지 않는 범위 내에서의 복제를 허용합니다.
   ② 본인의 논문을 디지털화하여 인터넷 등 정보통신망을 통한 논문의 일부 또는 전부의 복제·배포 및 전송 시 무료로 제공하는 것에 동의합니다.
2. 개인(저작자)의 의무
   본 논문의 저작권을 타인에게 양도하거나 또는 출판을 허락하는 등 동의 내용을 변경하고자 할 때는 소속대학(원)에 공개의 유보 또는 해지를 즉시 통보하겠습니다.
3. 서울대학교의 의무
   ①서울대학교는 본 논문을 외부에 제공할 경우 저작권 보호장치(DRM)를 사용하여야 합니다.
   ②서울대학교는 본 논문에 대한 공개의 유보나 해지 신청 시 즉시 처리해야 합니다.

논문제목 : Analysis of Retinal Proteome in Oxygen-induced Retinopathy

학위구분 : **석사 □ · 박사 ■**
학 과 : 의학과
학 번 : 2009-30505
연 락 처 :
저 작 자 : 김 상 진 (인)

제 출 일 : 2013년 1월 일

서울대학교총장 귀하

Abstract

Analysis of Retinal Proteome in Oxygen-induced Retinopathy

Sang Jin Kim
Medicine (Ophthalmology)
The Graduate School
Seoul National University

To identify proteins that are involved in the molecular mechanisms of oxygen-induced retinopathy (OIR), a well-established model of blinding ischemic retinopathy, the retinal proteome was quantitatively analyzed in a mouse model of OIR. OIR was induced by exposing C57BL/6 mice on postnatal day 7 (P7) to 75% hyperoxia for 5 days, followed by 5 days in room air. Retinas from mice on P12 and P17, the hyperoxic and hypoxic phases, respectively, and control groups were examined using isobaric tags for relative and absolute quantitation (iTRAQ) and nano-LC-ESI-MS/MS. In total, 1422 retinal proteins were identified—699 from the iTRAQ experiment and 1074 by nano-LC-ESI-MS/MS. Compared with control retinas in the iTRAQ study, OIR retinas upregulated and downregulated 21 and 17 proteins, respectively, in P17 retinas and 25 and 14 proteins, respectively, in P12 retinas. Of the differentially expressed proteins, the retinal expression of crystallin proteins, Müller cell-associated proteins, neurodegeneration-associated proteins, and angiogenesis-associated proteins, such as 150-kDa oxygen-regulated protein (ORP150) were analyzed. ORP150 colocalized to the neovascular tufts, and knockdown

of ORP150 by siRNA decreased the levels of secreted VEGF in cultured retinal pigment epithelial cells. Moreover, intravitreal administration of siRNA targeting ORP150 significantly reduced the retinal neovascularization in OIR. In conclusion, our proteomic discovery method, coupled with targeted approaches, revealed many proteins that were differentially regulated in the mouse model of OIR. These proteins, including ORP150, are potential novel therapeutic targets for the treatment of proliferative ischemic retinopathy.

* This work is published in"Journal of Proteome Research"(Sang Jin Kim, Jonghwa Jin, Young Joo Kim, Youngsoo Kim, Hyeong Gon Yu. Retinal proteome analysis in a mouse model of oxygen-induced retinopathy. J Proteome Res. 2012;11:5186-203).

Keywords: oxygen induced retinopathy, iTRAQ, angiogenesis, crystallin, 150-kDa oxygen-regulated protein, Müller cell.
Student Number : 2009-30505

Contents

List of Tables

List of Figures

Introduction

Ischemic retinopathies, such as retinopathy of prematurity, proliferative diabetic retinopathy, and retinal vein occlusion, are major causes of permanent blindness.[1-3] They present as abnormal retinal vascular proliferation, which leads to blinding complications, such as hemorrhage and retinal detachment.

Several proangiogenic factors, including vascular endothelial growth factor (VEGF), insulin-like growth factor, and erythropoietin, and antiangiogenic factors, such as angiostatin and pigment epithelium-derived factor, have been identified, the imbalance of which mediates the pathogenesis of retinopathy.[1,4-8] In addition, proteins that are related to inflammation, oxidative stress, and neuronal dysfunction might contribute to the molecular pathogenesis of ischemic retinopathy.[9-12] However, the pathogenic mechanisms of ischemic retinopathy are not fully understood, rendering the treatment challenging.

Proteomic platforms are useful for making unbiased discoveries of pathogenic factors that mediate ischemic retinopathy. Using isobaric tags for relative and absolute quantitation (iTRAQ), in which reporter ions are differentially and isotopically labeled, the relative concentrations of specific peptides can be determined from mixtures of complex proteins.

The iTRAQ technique has several advantages, such as its multiplexing capability, enabling simultaneous quantitation; relatively small intraexperimental variability; and higher sensitivity compared with other commonly used quantitation techniques, such as isotope-coded affinity tags and 2-dimensional difference in-gel electrophoresis.[13] Through proteomic methods that incorporated 2-dimensional gel-based proteomic analysis, iTRAQ, and nano-LC-ESI-MS/MS, several factors that might be related to the pathogenesis of diabetic retinopathy were identified in vitreous and

plasma samples from diabetic patients and retinal tissues from diabetic animal models.[14-20]

Oxygen-induced retinopathy (OIR) is a well-established animal model of blinding ischemic retinopathy.[1,21-24] In the mouse model of OIR, neonatal mice are exposed to 75% hyperoxia from the postnatal day7 (P7) until P12. During this phase, hyperoxic environment inhibits the retinal vessel growth and causes the degeneration of the existing blood vessels, which are apparent at P12. On returning to room air, the vascular retina becomes relatively hypoxic and triggers the production of angiogenic factors, which effects pathological angiogenesis. During the hypoxic phase, neovascularization develops and reaches its maximum at P17. Because the OIR model shares end results with human ischemic retinopathies — ie, capillary loss and subsequent hypoxia-induced retinal neovascularization — it has been used widely to examine the pathogenic mechanisms of ischemic retinopathies and evaluate new therapeutic agents.[1,21-24] Thus, a proteomic study that uses the OIR model might identify candidate proteins that are involved in the mechanisms of ischemic retinopathy, thereby constituting novel therapeutic targets. However, the retinal proteome in OIR has not been studied comprehensively.

In this study, to identify proteins that are related to the molecular mechanisms of OIR, we profiled the retinal proteome of the OIR mouse model by nano-LC-ESI-MS/MS and quantified retinal proteins by iTRAQ labeling, coupled with LC-MS/MS. Of the proteins that were differentially expressed between control and OIR retinas, we selected proteins that were suspected of being associated with angiogenesis, retinal vascular changes, and neurodegeneration in OIR, and performed a detailed characterization using targeted methods.

One such protein, ORP150, was upregulated in OIR and colocalized to neovascular tufts. The knockdown of ORP150 by siRNA downregulated secreted VEGF levels in cultured retinal pigment

epithelial cells, implicating ORP150 in pathological retinal angiogenesis. Moreover, intravitreal administration of siRNA targeting ORP150 significantly reduced the retinal neovascularization. Overall, the proteomic discovery method, coupled with targeted approaches, revealed many differentially regulated proteins in the mouse model of OIR. These proteins, including ORP150, might be novel therapeutic targets for the treatment of proliferative ischemic retinopathy.

Materials and Methods

OIR mouse model

OIR was induced as described.[21,23] Briefly, newborn C57BL/6 mice were randomly assigned to experimental and control groups. On postnatal Day 7 (P7), the pups and their nursing mothers were placed in a 75% oxygen atmosphere. The oxygen concentration was maintained with a Pro-Ox110 oxygen controller (Bio-Spherix, Redfield, NY, USA). To serve as a CO2 quencher, 50g of soda lime was placed at the bottom of the chamber. The pups were returned to room air on P12. The mice were sacrificed on P12 and P17, and the eyes were enucleated. The control groups were subjected to room air until sacrifice. Mice that weighed less than 6 g on P17 were excluded from the analysis due to possible alterations in vascular phenotype.[23] Mice were divided into 4 groups: control groups that were enucleated on P12 (P12C) and P17 (P17C) and OIR groups that were enucleated on P12 (P12) and P17 (P17). To confirm the development of OIR, retinal flat mounts (n=8 eyes per groups) and paraffin-embedded retinal sections (n=10 eyes per groups) were generated. After staining the retinal vessels with TRITC-labeled BS-1 lectin (L5264, Sigma Aldrich, St. Louis, MO, USA), we evaluated the retinal vaso-obliteration in P12 retinas and vascular regrowth and neovascularization in P17 retinas by confocal microscopy (LSM 500, Carl Zeiss MicroImaging GmbH, Germany). All animal experiments were conducted per the ARVO Statement for the Use of Animals in Ophthalmic and Vision Research and approved by the IACUC of Biomedical Research Institute, Seoul National University Hospital.

Retinal protein extraction

After enucleation, the retinas were isolated carefully under a

dissecting microscope. After the cornea was secured, the sclera was peeled away toward the optic nerve with dissecting forceps. The sclera, optic nerve, and retinal pigment epithelium were then removed. Finally, we removed the retina from the lens and vitreous, carefully ensuring the lens integrity.

Proteins were extracted from the 4 groups of retinas (n=22 eyes per group). The retinas in each group were pooled and homogenized in ice-cold PBS with protease inhibitor cocktail (Roche Complete Mini Tablets, Roche Applied Sciences, Indianapolis, IN, USA) by sonication and freeze-thaw lysis method. Protein concentrations were measured with Pierce BCA reagent (Thermo Scientific, Rockford, IL, USA). The 4 groups of pooled protein samples were used for iTRAQ experiment, LC-ESI-MS/MS analysis, and western blot analysis.

iTRAQ experiment [1)]

The iTRAQ technique was used to compare protein expression profiles in OIR tissues between P12 and P12C, between P17 and P17C, and between P17 and P12, allowing us to perform a comprehensive analysis of differential proteome expression by comparing the 4 iTRAQ reporter ions. iTRAQ labeling and fractionation were performed as described.[25,26]

One hundred micrograms of protein was labeled with iTRAQ reagents, and the proteins were reduced, alkylated, digested, and labeled per the manufacturer's instructions (Applied Biosystems, Foster City, CA, USA). For iTRAQ labeling, the 4 groups of retinas—P12C, P17C, P12, and P17—were labeled with iTRAQ reagents 114, 115, 116, and 117. The iTRAQ experiments were performed in triplicate with the same samples. The labeled iTRAQ samples were separated into 45 fractions by strong cation exchange (SCX)

1) iTRAQ 분석과 LC-ESI-MS/MS 분석은 공동연구자인 서울대학교 의학과 박사과정 진종화에 의해 수행됨.

chromatography on an Agilent 1100 (Agilent Technologies, Palo Alto, CA, USA) with an SCX column (4.6 mm ID x 100 mm, 5 μm, 200A, PolyLC, Columbia, MA, USA).

LC-MS/MS experiments were performed as described.[25,26] LC-MS/MS was performed using an integrated system, which comprised an autosampler switching pump and a micropump (Tempo Nano LC system; Applied Biosystems) with a hybrid quadrupole-TOF LC-MS/MS spectrometer (QStar Elite; Applied Biosystems) that was equipped with a nanoelectrospray ionization source (Applied Biosystems).

The data analysis was performed as described.[25,26] Data file processing, protein identification, and relative abundance quantitation were performed using ProteinPilot v.2.0.1 and the Paragon algorithm. Database searches were performed against the mouse database (mouse combined_KBMS5.0.20050302.fasta was provided by Applied Biosystems).

LC-ESI-MS/MS analysis [1)]

Retinal proteins were also analyzed by LC-MS/MS on an EasyLC (Proxeon, Odense, Denmark), which was coupled to a high-throughput tandem mass spectrometer (LTQ Velos, Thermo, Waltham, MA, USA) that was equipped with a nanoelectrospray device and fitted with a 10-μm fused silica emitter tip (New Objective, Woburn, MA, USA).

All MS/MS spectra from LTQ Velos were analyzed using SEQUEST (Thermo Fisher Scientific, San Jose, CA, USA; version v.27, rev. 11), using the mouse database Uniprot-mouse.FASTA (147,548 entries).

Scaffold version Scaffold_3_00_03 (Proteome Software Inc., Portland, OR, USA) was used to validate all MS/MS-based peptide and protein identifications. We selected peptides with greater than 95.0%

probability, as specified by the Peptide Prophet algorithm.[27] Moreover, we used specific database search engine thresholds to validate the MS/MS-based peptides. SEQUEST identifications required at least deltaCn scores of greater than 0.10 and XCorr scores of greater than 1.8, 2.8, and 3.8 for singly, doubly, and triply charged peptides, respectively. All identified proteins were satisfied by greater than 95.0% probability and at least 2 identified peptides.[28]

Immunofluorescence staining

Eyes (n=10 eyes per group) were enucleated, immersed in 4% paraformaldehyde for 24 hours, and embedded in paraffin. Four-micron-thick serial sections were prepared from paraffin blocks. After deparaffinization and hydration, sections were incubated for 1 hour in a blocking solution that was obtained from the same species in which the secondary antibody was developed. The slides were incubated with primary antibodies, as detailed in Table 1.

After being washed with PBS, the slides were incubated for 1 hour with Alexa Fluor 488 goat anti-mouse IgG (1:400, Invitrogen Molecular probes, Eugene, OR, USA), Alexa Fluor 488 goat anti-rabbit IgG (1:400, Invitrogen Molecular probes), or Alexa Fluor 555 donkey anti-goat IgG (1:700, Invitrogen Molecular probes). Blood vessels were stained with TRITC-labeled BS-1 lectin (L5264, Sigma Aldrich), and cell nuclei were counterstained with DAPI. The stained sections were examined by confocal microscopy.

Western blot

Each protein sample (10-30 μg) was separated on a 4-12% Bis-Tris gel (NuPAGENovex, Invitrogen) and transferred onto a PVDF membrane (Millipore, Billerica, MA, USA). The membranes were blocked with 5% skim milk in TBS-T (20 mM Tris-base, 150 mM NaCl, pH 7.4) and incubated with primary antibodies, rabbit

anti-crystallin αB (1:500), rabbit anti-crystallin αB P-Ser-59 (1:500), rabbit anti-ORP150 (1:1000), rabbit anti-carbonic anhydrase II (CA II, 1:25,000), and rabbit anti-carbonic anhydrase XIV (1:100). After a wash step, anti-rabbit IgG-alkaline phosphatase secondary antibody (1:20,000, Sigma Aldrich), was added for 1 hour at room temperature. The antibody reactions were visualized using Fast BCIP/NBT alkaline phosphatase substrate (Sigma Aldrich).Western blots for crystallin α B, crystallin αB P-Ser-59, CA II, and ORP150 were performed in triplicate. The western blots were scanned, and relative band densities were calculated using ImageJ (National Institutes of Health, Bethesda, MD, USA). The values between the groups were compared with the Mann-Whitney U test using SPSS for Windows (version 18.0, SPSS Inc., Chicago, IL, USA).

ELISA of VEGF from ORP150 siRNA-treated ARPE-19 cell line

ARPE-19 cells (American Type Culture Collection, Rockville, MD, USA), a spontaneously immortalized human retinal pigment epithelial cell line, were maintained in DMEM-F12 medium, containing 10% fetal bovine serum (FBS). We seeded a 6-well culture plate with 2 x 10^5 cells per well in 2 ml antibiotic-free DMEM-F12 medium that was supplemented with FBS.

ARPE-19 cells were transfected with control siRNA (sc-37007, Santa Cruz Biotechnology, Santa Cruz, CA, USA) or ORP150 siRNA (sc-96695, Santa Cruz Biotechnology), a pool of 3 target-specific 19-25-nt siRNAs that were designed to knock down gene expression, per the manufacturer's protocol. Briefly, ARPE-19 cells were incubated at 37°C in a CO_2 incubator until the cells were 60% to 80% confluent. The siRNA transfection reagent mixture was added to the cells to 500nM or 1 μM. After a 6-hour incubation, the medium was replaced with fresh DMEM-F12 medium.

After an additional incubation for 24 hours, the supernatants of the cultures were harvested to measure secreted VEGF levels using a human VEGF ELISA kit (Thermo scientific) per the manufacturer's protocol. To validate the knockdown of ORP150, proteins that were extracted from the cell lysates were analyzed by western blot for ORP150 using rabbit anti-ORP150 (1:1000, Epitomics, Burlingame, CA, USA). The western blots were scanned, and relative band densities were calculated using ImageJ.

Intravitreal administration of siRNA against ORP150 in OIR

To assess the antiangiogenic effect of ORP150 inhibition, we intravitreally injected ORP150 siRNA (550ng/1㎕, sc-96695, Santa Cruz Biotechnology) diluted in lipid-based in vivo transfection reagent (Altogen Biosystems, Las Vegas, NV, USA) in one eye and control siRNA (sc-37007, Santa Cruz Biotechnology, Santa Cruz, CA, USA) in the remaining eye at P12 in a mouse model of OIR. At P17, to validate the knockdown of ORP150, retinal proteins were extracted (n=6 eyes per group) and analyzed by western blot for ORP150, using rabbit anti-ORP150 (1:1000, Epitomics, Burlingame, CA, USA). Three independent western blot-based measurements were performed. For quantitative and qualitative assessment of the effect of ORP150 siRNA on neovascularization, at P17, eyes (n=12 eyes per group) were enucleated and fixed in 4% paraformaldehyde. Six eyes per group were embedded in paraffin and quantitation of neovascularization was performed, as previously described.[29] In brief, after staining with hematoxylin and eosin, we counted the vascular lumens on the vitreal side of the internal limiting membrane in at least 10 sections from each eye by two independent observers. For qualitative assessment of retinal neovascularization at P17, retinal flat mounts (n=6 eyes per group) were generated. After staining the

retinal vessels with TRITC-labeled BS-1 lectin, retinal flat mounts were examined by a confocal microscopy and were compared between ORP150 siRNA treated and control siRNA treated eyes.

In addition, immunofluorescence staining was also performed with primary antibodies against vimentin and glutamine synthetase (Table 1) to evaluate the changes in Müller glial cells after ORP150 knockdown. Also, density of retinal ganglion cells were determined from the hematoxylin and eosin stained retinal sections as previously described with some modifications.[30,31] In brief, photomicrographs were captured at 0.5 and 1.5 mm from the center of the optic nerve head, which represents central avascular retina and peripheral retina with neovascularization, respectively. Cells in the ganglion cell layer were counted by two independent observers and reported as a density of retinal ganglion cells (cells/mm). The values used were averaged from six measurements in each eye.

Results

OIR mouse model

The generation of the OIR model was confirmed by histological analysis of the retinal flat mounts and retinal sections. By confocal micrography, flat-mounted retina from the mouse model of OIR showed vaso-obliteration in the central retinal area in the P12 samples and neovascularization in the P17 samples (Figure 1). Additionally, neovascular tufts on the vitreal side of the internal limiting membrane were observed in P17 samples, in contrast to the normal retinal vasculature of the P17 control (Figure 1).

Identification of differential proteomes using iTRAQ

In total, 699 proteins from 2437 peptides in the 3 combined iTRAQ experiments at a minimum confidence level of 95% were identified (unused ProtScore>1.3). One hundred eithty-two proteins (unused ProtScore>1.3) were common to all 3 iTRAQ experiments at a minimum confidence level of 95% using 3 pooled retina samples. The labeling efficiency was greater than 98% in these iTRAQ experiments (data not shown).

To obtain bond fide iTRAQ results, possible variations in the replicate iTRAQ experiments must be identified and minimized. In calculating the cutoff threshold for meaningful fold-changes over experimental errors, the variations between experimental replicates were considered to be actual variations in the 3 iTRAQ experiments. Consequently, the 3 iTRAQ experiments identified 699 proteins, but the number of commonly identified proteins was 182.

Using the following selection criteria—containing more than 2 unique peptides (>95%), a p-value <0.05, and error factor (EF)<2—in the P12 versus P12C, P17 versus P17C, and P12 versus P17 OIR tissue comparisons, 165 proteins were quantitated in the 3 iTRAQ

experiments. These proteins were used initially to determine the experimental variations and confirm the cutoff threshold for meaningful fold-changes.[32]

Based on the 3-standard deviation model, we concluded that a fold-change of >1.20 or <0.83 was a meaningful cutoff that reflected actual differences in protein expression between the 116/114, 117/115, and 117/116 reporter ions. Ultimately, 72 proteins had a p-value <0.05, EF<2, more than 2 unique peptides with >95% confidence level, and expression that modulated by >±1.20-fold in all 3 iTRAQ experiments.

Differential retinal proteomes at P12 of OIR

Of the 72 quantified proteins from the iTRAQ experiment, 39 proteins were differentially expressed in P12 retinas (116 reporter) compared with P12C (114 reporter), comprising 25 upregulated and 14 downregulated proteins (Table 1).

Differential retinal proteomes at P17 of OIR

In the P17 retinas (117 reporter), 38 differentially expressed proteins—21 upregulated and 17 downregulated—were identified versus P17C (115 reporter) (Table 1).

Comparison of retinal proteomes between hyperoxic (P12) and hypoxic retinas (P17)

On comparison of the P17 and P12 proteomes, 36 differentially expressed proteins — 21 upregulated and 15 downregulated — were identified in P17 retinas (Table 1).

Cluster analysis of differentially expressed proteomes

Next, we analyzed the protein expression patterns over time, based on rises and declines in protein levels at P12 and P17—the hyperoxic and hypoxic phases, respectively. In the subclustering analysis, we categorized major patterns of up- and downregulation into 4 subclusters: subclusters 1 (upregulated in P17), 2 (upregulated in P12 and P17), 3 (upregulated in P12), and 4 (downregulated in P17).

Subcluster 1 was composed of 7 proteins—phosphoglycerate kinase 1 (PGK1), microtubule-associated protein 1 B (MAP1B), crystallin βA2, crystallin βB2, recoverin, basigin precursor, and mKIAA0193—that were upregulated in P17 (Figure 2).

Subcluster 2 comprised 10 proteins—creatine kinase B, 14-3-3 protein zeta/delta, serum albumin precursor, acyl-CoA-binding protein, transketolase, malate dehydrogenase 2, crystallin αA, neddylin, isocitrate dehydrogenase, and crystallin αB—that rose in expression in P12 and P17 (Figure 2).

Subcluster 3 contained 6 proteins—s-arrestin, Ubb protein, non-histone chromosomal protein HMG-17, vesicle-docking protein, trypsinogen 16, and dihydropyrimidinase-related protein-3—that were upregulated in P12 but downregulated in P17 retinal tissue (Figure 2).

Subcluster 4 comprised 6 proteins—histone 1, histone H2b, NRAA, excitatory amino acid transporter 1, 40S ribosomal protein, and neural cell adhesion molecule—that were downregulated in P17 retinal tissue (Figure 2).

Identified proteins from LC-MS/MS analysis using LTQ Velos

To identify specific proteins in P12 and P17 OIR tissue, we used a complementary LC-ESI-MS/MS analytical platform with LTQ Velos. In total, 1074 retinal proteins were identified in P12C, P17C, P12, and P17 retinal tissue — 364 proteins were common between P12C and P12 retinal tissue, and 34 and 578 proteins were unique in P12C and

P12 retinas, respectively. Four hundred ninety-six proteins were common between P17C and P17 retinal tissue, and 270 and 135 proteins, respectively, were unique. Forty-three and 138 proteins were unique in P17 and P12 retinas, respectively.

In this LC-ESI-MS/MS analysis, 723 proteins were newly identified compared with the iTRAQ results. Thus, 1422 proteins were identified using iTRAQ and the LTQ Velos.

Selection of proteins of interest

The nano-LC-ESI-MS/MS and iTRAQ experiment of OIR retinal tissue implicated certain changes in the retinal proteome as therapeutic targets for further study with regard to their function in angiogenesis, vascular changes, and neurodegeneration. Six proteins—crystallin αA, crystallin αB, ORP150, PGK1, lens epithelium-derived growth factor (LEDGF/Psip1), and excitatory amino acid transporter 1 (Slc1a3/EAAT-1/GLAST)—were selected by iTRAQ, and 3 proteins—CA II, CA XIV, and crystallin βS—were selected by LTQ analysis. To examine their localization in the OIR retina, we examined retinal sections from control and OIR retinas by immunohistochemistry.

Retinal expression of crystallin αA, αB, and βS

The nano-LC-ESI-MS/MS and iTRAQ experiments identified crystallin αA and αB in control and OIR retinas. The iTRAQ experiments demonstrated that crystallin αA and αB were upregulated to a greater extent in OIR P17 than in OIR P12 retinas. Crystallin αA was immunoreactive in all retinal layers in control and OIR retinas, throughout the Müller cells (Figure 3). In OIR P17 retinas, there was intense immunoreactivity of crystallin αA in the ganglion cell layer (GCL) and inner nuclear layer (INL) (Figure 3).

Positive immunoreactivity for crystallin αB was observed in the ganglion cell layer/nerve fiber layer (GCL/NFL), inner plexiform layer

(IPL), INL, and outer nuclear layer (ONL) in control retinas (Figure 4). In OIR P12 and P17 retinas, crystallin αB immunoreactivity increased in all retinal layers (Figure 4). In OIR P17 retinas, the signal intensity rose, especially in the inner retinal surface and ONL. By western blot, retinal expression of crystallin αB was significantly up-regulated in P12 and P17, compared with the control retinas (Figure 4).

The chaperone activity of crystallin αB is regulated by its phosphorylation, particularly at Ser59.[33] In OIR P12 and P17 retinas, the immunoreactivity of crystallinαB P-Ser-59 was robust in the GCL/NFL (Figure 4). Higher-magnification images of double immunolabeling of crystallin αB P-Ser-59 with TRITC-labeled BS-1 lectin showed double-positive but weaker immunoreactivity in the neovascular tufts than in the GCL/NFL. By western blot, the retinal expression of crystallin αB P-Ser-59 was also significantly up-regulated in P12 and P17, compared with the control retinas (Figure 4).

Crystallin βS was identified by nano-LC-ESI-MS/MS in all 4 groups. In the retinal sections, crystallin βS immunoreactivity rose in the ONL of P12 and P17 OIR retinas (Figure 3).

Retinal expression of proteins predominantly in Müller glial cells

Retinal expression of glial fibrillary acidic protein (GFAP), a marker for astrocytes and activated Müller glial cells, increased in OIR P17 retinas (Figure 5). Additionally, immunoreactivity for vimentin and glutamine synthetase, markers of Müller cell gliosis, rose in the distal branches of Müller cells in OIR P17 retinas compared with control and OIR P12 retinas (Figure 5).

Nano-LC-ESI-MS/MS identified CA II and CA XIV, 2 isoenzymes of CA, in the retina.[34] To measure the retinal expression of CAII and

CAXIV, we performed western blot and immunohistochemistry. Quantitation of CA II by western blot showed that CA II was significantly up-regulated in the OIR P12 retina than in the control retinas at P12 and P17 (Figure 5). Also, CA II in the OIR P17 retina was more up-regulated than in the OIR P12 retina and normal control retinas (Figure 5). At P17, retinal CA II expression increased in the NFL/GCL, INL, and ONL, colocalizing with markers of Müller glial cells, such as glutamine synthetase (Figure 5) and vimentin (Figure 6). CA II immunoreactivity was prominent in the distal branches of Müller cells on P17. In contrast to CA II, there was no difference in CA XIV expression by western blot between OIR and control tissues (Figure 5). CA XIV was immunoreactive in all retinal layers, especially in the internal limiting membrane (ILM), outer plexiform layer (OPL), the inner aspect of the subretinal space, and the RPE layer, with similar patterns in all groups (Figure 5).

In the iTRAQ experiment, EAAT-1, a major glutamate transporter of Müller glial cells, was downregulated in OIR P12 and P17 retinas (Figure 2). Positive immunoreactivity for EAAT-1 was observed in all retinal layers, particularly the IPL and OPL, but there was no difference between OIR and control retinas (Figure 5).

Retinal expression of PGK1 and ORP150

In the iTRAQ experiment, PGK1 was upregulated in OIR P17 retinas compared with OIR P12 and control P17 retinas (Figure 6). PGK1 was immunoreactive in all retinal layers and colocalized with the neovascular tufts (Figure 7).

By nano-LC-ESI-MS/MS, ORP150 was expressed in OIR P12 and P17 retinas. Additionally, in the iTRAQ experiment, ORP150 appears in all 4 groups with 1 identified peptide. Although only 1 peptide was identified, ORP150 levels increased greater than 1.4-fold by iTRAQ in P12 and P17 compared with P12C and P17C, respectively.

Quantitation of ORP150 by western blot showed that ORP150 was significantly up-regulated in OIR P12 and P17 retinas, compared with that of the control retinas at P12 and P17 (Figure 8). In the retinal sections, ORP150 immunoreactivity was detected in the perinuclear region of the GCL, INL, and RPE layer (Figure 8). Notably, in OIR P17 retinas, ORP150 immunoreactivity was intense in the inner retinal layers and colocalized with the neovascular tufts (Figure 8). ORP150 immunoreactivity was not colocalized with immunoreactivity of Iba-1, a microglical marker (Figure 9).

Retinal expression of LEDGF

In the iTRAQ experiment, LEDGF was downregulated in P17 compared with P12. LEDGF was immunoreactive in all retinal nuclear layers but did not differ between groups (Figure 3).

Function of ORP150 in VEGF secretion in retinal pigment epithelium

To examine the function of ORP150 in retinal angiogenesis, the secretion of VEGF by retinal pigment epithelium (RPE) cells was measured after downregulation of ORP150 expression. By western blot, ORP150 expression declined on transfection with ORP150 siRNA (Figure 10). Further, secreted VEGF levels by ARPE-19 cells fell significantly 24 hours after transfection ($P<0.01$, t-test) (Figure 10).

The effect of siRNA targeting ORP150 on retinal neovascularization in OIR

Quantitation of ORP150 by western blot showed that intravitreally administered siRNA targeting ORP150 substantially down-regulated the retinal expression of ORP150 (Figure 11). Both qualitative and quantitative assessment of the retinal neovascularization showed that

the intravitreally administered siRNA targeting ORP150 significantly reduced the retinal neovascularization in a mouse model of OIR (Figure 11). We also investigated whether the anti-angiogenic effect was associated with Müller cell activation. However, immunoreactivity for vimentin and glutamine synthetase, markers for Müller cell gliosis, was not different between ORP150 siRNA-treated retina and control siRNA-treated retina (Figure 12). Further, to investigate whether the anti-angiogenic effect of siRNA targeting ORP150 was associated with degeneration of retinal ganglion cells, density of retinal ganglion cells were determined. In hematoxylin and eosin stained retinal sections, densities of retinal ganglion cells at 0.5 and 1.5 mm from the center of the optic nerve head showed no statistically significant difference between control and ORP150 siRNA injected eyes ($P>0.05$, Figure 13).

Table 1. Primary antibodies used for immunohistochemistry

Primary Antibody	Source	Product No.	dilution
Rabbit anti-Crystallin αA	Enzo	ADI-SPA-221	1:100
Rabbit anti-Crystallin αB	Enzo	ADI-SPA-223R	1:100
Rabbit anti-Crystallin αB P-Ser59	Enzo	ALX-210-411	1:100
Rabbit anti-Crystallin βS	Abcam	ab80040	1:50
Rabbit anti-LEDGF	Cell signaling	#2088	1:25
Rabbit anti-PGK1	LifeSpan	LS-C98055	1:25
Rabbit anti-CA2	Abcam	ab6621	1:700
Goat anti-CA2	Santa Cruz	sc-17246	1:50
Rabbit anti-CA14	Santa Cruz	sc-25602	1:200
Goat anti-Vimentin	Millipore	AB1620	1:100
Rabbit anti-GFAP	DakoCytomation	Z0334	1:300
Rabbit anti-GS	Abcam	ab49873	1:10000
Rabbit anti-EAAT1	Abcam	Ab416	1:50
Rabbit anti-ORP150	Epitomics	3905-1	1:250
Goat anti-Iba-1	Abcam	Ab5076	1:100

Table 2. Differentially expressed retinal proteins, as quantified by iTRAQ at P12 and P17 in OIR.

Values were derived from a pooled sample of OIR retinas, and the iTRAQ experiment was performed in triplicate. Proteins were grouped according to the day that had the greatest upregulation or downregulation relative to each control. Increases in expression are marked in red, and decreases are shown in blue.

Accession No.	Gene name	Protein name	Fold-change		
			P12 : P12C (116:114)	P17:P17C (117 : 115)	P17:P12 (117 : 116)
Proteins up- or down-regulated at P12 compared with P12C					
spt|Q62188	Dpysl3	Dihydropyrimidinase-related protein	1.72±0.01	1.02±0.01	0.78±0.01
spt|P31786	Dbi	Acyl-CoA-binding protein	1.61±0.01	1.48±0.01	0.75±0.01
trm|Q8BMU7	Etfa	Electron transfer flavor protein alpha	1.46±0.15	1.28±0.02	0.94±0.02
cra|mCP99343	tpm1	tropomyosin 1, alpha	1.45±0.18	1.15±0.09	0.80±0.09
spt|P46460	Nsf	Vesicle-fusing ATPase	1.45±0.06	0.90±0.02	0.74±0.03
trm|Q9D6A4	Ttr	Putative uncharacterized protein	1.40±0.09	1.10±0.01	0.82±0.01
spt|P20443	Sag	S-arrestin	1.37±0.06	1.18±0.02	0.96±0.02
cra|mCP114716	Cln5	hypothetical protein	1.33±0.11	1.04±0.01	0.83±0.01
trm|Q9Z1R9	Prss1	Trypsinogen 16	1.32±0.02	1.05±0.01	0.75±0.01
trm|Q91WE7	Uso1	Vesicle docking protein	1.31±0.01	1.07±0.01	0.82±0.01
cra|mCP9707.2	groL1	RIKEN cDNA 2310046H11 gene	1.31±0.01	1.05±0.01	0.71±0.01
spt|O88844	Idh1	Isocitrate dehydrogenase [NADP] cytoplasmic	1.30±0.01	1.25±0.04	0.82±0.05
trm|Q9DA96	1700016M24Rik	Hypothetical ARM repeat structure-containing protein	1.3±0.03	1.13±0.01	0.71±0.02

trm|Q792Y8	Gm10334	Trypsinogen 15	1.28±0.02	0.98±0.01	0.76±0.01
spt|P29595	Nedd8	Neddylin	1.28±0.01	1.22±0.01	0.89±0.01
spt|P63101	Ywhaz	14-3-3 protein zeta/delta	1.24±0.05	1.20±0.01	0.97±0.02
cra|mCP42740.1	pyrE	hypothetical protein	1.23±0.04	1.17±0.01	0.94±0.01
trm|Q91XV3	Basp1	22 kDa neuronal tissue-enriched acidic protein	1.23±0.01	1.00±0.01	0.83±0.01
trm|Q6NZC5	Ubb	Ubb protein	1.21±0.01	0.88±0.01	0.78±0.01
trm|Q8BFZ3	Actbl2	ACTIN, CYTOPLASMIC TYPE 5 homolog	0.80±0.05	0.96±0.02	1.12±0.03
trm|Q9CX86	Hnrnpa0	Heterogeneous nuclear ribonucleo protein A0	0.78±0.01	1.00±0.02	1.20±0.02
rf|NP_034851.1	Lmnb1	lamin B1	0.72±0.02	0.87±0.02	1.14±0.02
pir|S04585	Ncam	neural cell adhesion molecule	0.7±0.01	0.71±0.01	1.04±0.01
spt|P24547	Impdh2	Inosine-5'-monophosphate dehydrogenase 2	0.51±0.04	1.01±0.01	1.04±0.01

Proteins up- or down-regulated at P17 compared with P17C

cra|mCP74734	Cryba2	crystallin, beta A2	0.73±0.01	2.47±0.01	1.75±0.01
spt|P23927	Cryab	Alpha crystallin B chain	1.31±0.03	2.27±0.01	1.00±0.01
pir|A39757	Crybb2	beta-crystallin B2	1.02±0.03	1.83±0.03	1.35±0.04
pir|CYMSA	Cryaa	alpha-crystallin chain A	1.22±0.03	1.71±0.01	0.90±0.02
spt|P07724	Alb	Serum albumin precursor	1.34±0.02	1.50±0.01	1.03±0.02
spt|P28352	Apex1	DNA-(apurinic or apyrimidinic site) lyase	1.01±0.01	1.49±0.01	1.13±0.01
spt|P17742	Ppia	Peptidyl-prolyl cis-trans isomerase A	1.15±0.06	1.42±0.05	1.1±0.06
trm|Q5XJE7	Pgk1	Pgk1 protein	1.13±0.03	1.38±0.01	1.23±0.01
spt|P34057	Rcvrn	Recoverin	1.18±0.01	1.35±0.01	1.12±0.01
spt|P40142	Tkt	Transketolase	1.20±0.01	1.31±0.01	1.08±0.01
trm|Q8R1P0	Mdh2	Malate dehydrogenase 2, NAD	1.27±0.07	1.30±0.01	0.98±0.01
spt|Q04447	Ckb	Creatine kinase, B chain	1.25±0.01	1.27±0.01	0.89±0.01
dbj|BAC97894.1	Scrn1	mKIAA0193 protein	0.85±0.01	1.25±0.01	1.23±0.01

cra|mCP113378	Ssb	Sjogren syndrome antigen B	0.99±0.03	1.21±0.04	1.13±0.05
cra|mCP98175	Vmn1r171	NCAM polypeptide precursor	1.00±0.01	0.82±0.01	0.94±0.01
gb|AAH31728.1	Stxbp1	Stxbp1 protein	0.93±0.09	0.80±0.07	1.17±0.07
trm|Q91ZZ3	Sncb	Beta-synuclein	0.84±0.03	0.80±0.06	1.09±0.06
spt|P30681	Hmgb2	High mobility group protein 2	0.93±0.01	0.80±0.01	0.83±0.01
cra|mCP97064	DPYSL3	dihydropyrimidinase-like 3	0.80±0.01	0.8±0.01	1.16±0.01
trm|Q80TI5	Slc12a5	MKIAA1176 protein	0.88±0.04	0.79±0.02	1.12±0.03
spt|P60867	Rps20	40S ribosomal protein S20	0.97±0.01	0.79±0.01	0.83±0.01
trm|Q9QZQ8	H2afy	Histone macroH2A1.2 variant (MacroH2A1.2)	0.96±0.05	0.78±0.08	0.91±0.08
spt|P43275	Hist1h1a	Histone H1.1 (H1 VAR.3) (H1a)	0.99±0.01	0.74±0.03	0.92±0.04
spt|P43274	Hist1h1e	Histone H1.4 (H1 VAR.2) (H1e)	0.97±0.01	0.73±0.01	0.84±0.01
spt|P43276	Hist1h1b	Histone H1.5 (H1 VAR.5) (H1b)	0.92±0.04	0.68±0.01	0.84±0.01
rf|NP_056601.1	Hist1h1c	histone 1, H1c	0.88±0.01	0.66±0.01	0.82±0.02
spt|P56564	Slc1a3	Excitatory amino acid transporter 1	0.71±0.01	0.64±0.01	1.15±0.01
cra|mCP51905	MCA1905	Core histone H2A/H2B/H3/H4	0.74±0.01	0.63±0.01	0.90±0.01
trm|Q64478	Hist1h2bh	Histone H2b (Histone protein Hist1h2bh)	0.73±0.01	0.57±0.01	0.86±0.01

Proteins up- or down- regulated at P17 compared with P12

rf|XP_483976.1	Gapdh	similar to glyceraldehyde-3-phosphate dehydrogenase	0.64±0.05	1.06±0.08	1.62±0.08
trm|Q9CY54	Hbb-b1	Hemoglobin, beta adult major chain	0.93±0.02	1.33±0.07	1.56±0.08
cra|mCP51933.1	eno1	microtubule-associated protein 1 B	0.82±0.01	1.41±0.01	1.55±0.01
cra|mCP10468.2	Dnmt3b	aldolase 1, A isoform	0.95±0.01	1.19±0.02	1.42±0.02
spt|P35564	Canx	Calnexin precursor	0.72±0.01	0.92±0.10	1.39±0.10
trm|Q80WM3	Cplx4	Complexin IV	0.85±0.01	0.92±0.06	1.38±0.07
rf|XP_484728.1	Eno1	similar to Eno1 protein	0.96±0.01	1.14±0.02	1.34±0.02

rf|XP_134169.2	Slc25a4	solute carrier family 25	0.83±0.03	0.85±0.01	1.33±0.01
spt|Q60932	Vdac1	Voltage-dependent anion-selective channel protein 1	0.95±0.02	0.99±0.01	1.32±0.01
rf|XP_486749.1	Gapdh	similar to glyceraldehyde-3-phosphatedehydrogenase	1.14±0.07	1.12±0.14	1.27±0.15
spt|P46096	Syt1	Synaptotagmin-1	0.84±0.02	0.85±0.04	1.27±0.04
spt|P18572	Bsg	Basigin precursor	0.89±0.01	1.24±0.02	1.27±0.03
trm|Q6P5D0	Dpysl2	Dihydropyrimidinase-like 2	0.95±0.04	1.16±0.03	1.25±0.04
spt|P20152	Vim	Vimentin	0.99±0.02	1.16±0.02	1.25±0.03
spt|P16125	Ldhb	L-lactate dehydrogenase B chain	0.82±0.09	1.07±0.12	1.22±0.13
spt|Q61696	Hspa1a	Heat shock 70 kDa protein 1A	0.87±0.02	0.98±0.03	1.22±0.03
rf|NP_035229.2	Pkm2	pyruvate kinase 3	0.96±0.01	1.06±0.01	1.21±0.01
trm|Q99JF8	Psip1	Lens epithelium-derived growth factor a	1.02±0.01	0.84±0.02	0.79±0.03
spt|P09602	Hmgn2	Nonhistone chromosomal protein HMG-17	1.44±0.04	0.79±0.02	0.52±0.03

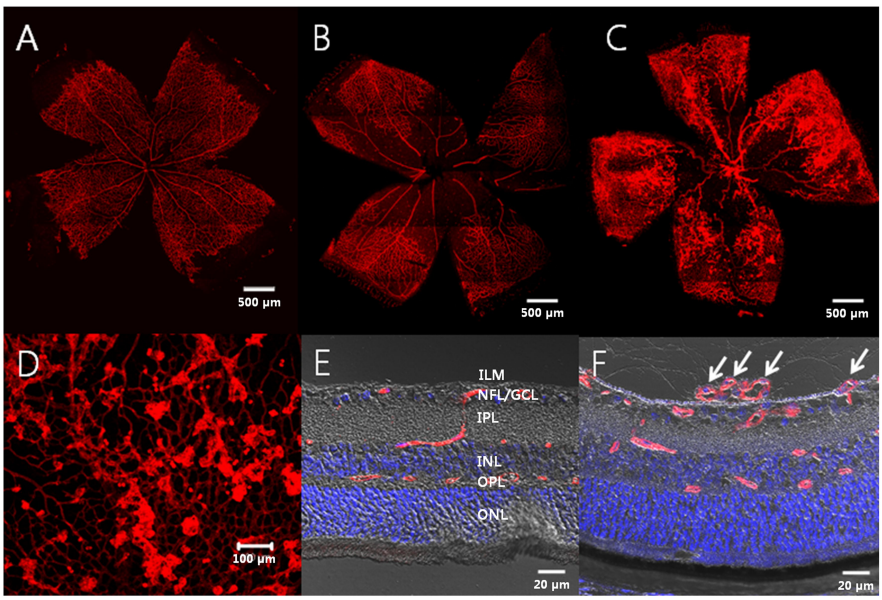

Figure 1. Confocal micrographs of flat-mounted and sectioned retinas from the mouse model of oxygen-induced retinopathy.

On postnatal Day 7 (P7) (A), when retinal vessels were not fully developed, mice were exposed to 75% oxygen, which effected significant vascular loss, shown in B, by P12. After returning to room air on P12, the avascular retina became hypoxic, triggering neovascularization, peaking on P17 (C and D). Note the neovascular tufts (red, arrows) on the vitreal side of the internal limiting membrane on P17 (F) in contrast to the normal retinal vasculature in the P17 control (red, E). In E and F, the nuclei were counterstained with DAPI (blue). ILM, internal limiting membrane; NFL/GCL, nerve fiber layer/ganglion cell layer; IPL, inner plexiform layer; INL, inner nuclear layer; OPL, outer plexiform layer; ONL, outer nuclear layer. Scale bars: A-C, 500 μm; D, 100 μm; E-F, 20 μm.

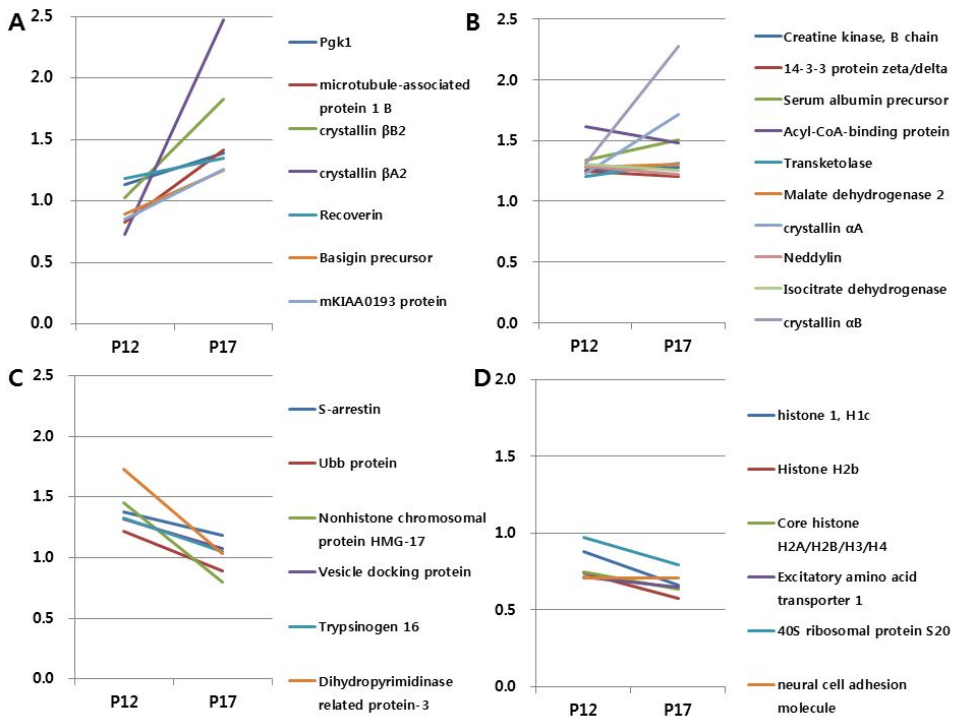

Figure 2. Cluster analysis of differentially expressed proteins in P12 and P17 retinas

The specific expression patterns were obtained by subclustering analysis, wherein 4 subclusters—1 (upregulated in P17, A), 2 (upregulated in both P12 and P17, B), 3 (upregulated in P12, C), and 4 (downregulated in P17, D)—were analyzed. Y-axis, fold change compared to each control.

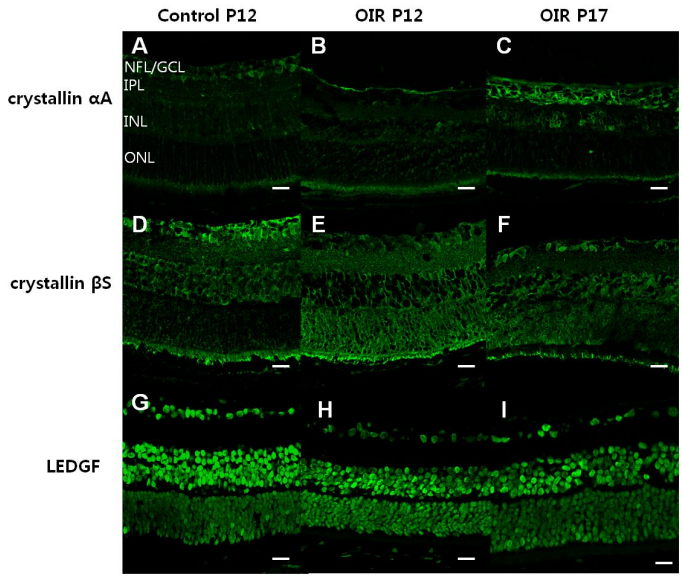

Figure 3. Immunolocalization of crystallin αA, crystallin βS, and lens epithelium-derived growth factor (LEDGF) in oxygen-induced retinopathy (OIR)

In OIR P17 retinas, intense immunoreactivity of crystallin αA was observed in the ganglion cell layer and inner nuclear layer compared with control and OIR P12 retinas (A-C). The immunoreactivity for crystallin βS was increased in the ONL of OIR P12 (E) and P17 retinas (F) compared with the control retina (D). The immunoreactivity for LEDGF, which was positive in all retinal nuclear layers, did not differ between groups (G-I). NFL, nerve fiber layer; GCL, ganglion cell layer; IPL, inner plexiform layer; INL, inner nuclear layer; OPL, outer plexiform layer; ONL, outer nuclear layer. Scale bar, 20 ㎛.

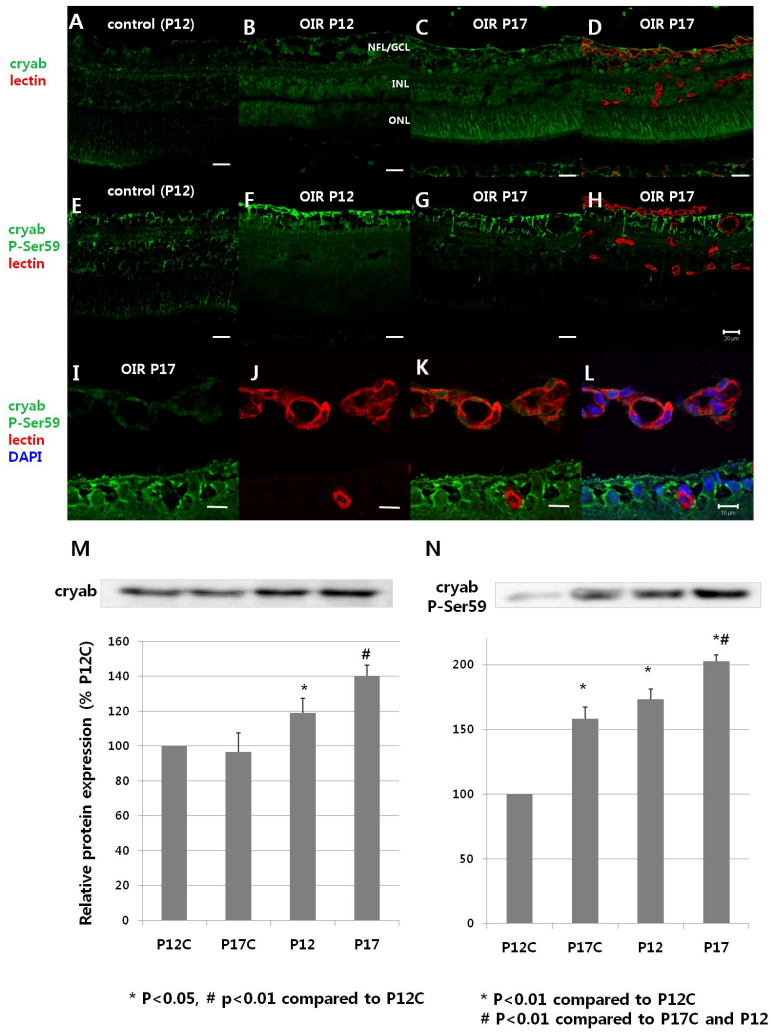

Figure 4. Immunolocalization and western blot analysis of crystallin αB in oxygen-induced retinopathy (OIR).

In control retinas, positive immunoreactivity for crystallin αB (green) was observed in the ganglion cell layer/nerve fiber layer (GCL/NFL), inner plexiform layer (IPL), inner nuclear layer (INL), and outer nuclear layer (ONL) (A). In OIR postnatal Day 12 (P12) and P17 retinas, the immunoreactivity for crystallin αB was increased (B-D). In OIR P17 retinas, the signal intensity was

increased in the inner retinal surface and ONL (C,D). In OIR P12 and P17 retinas, the immunoreactivity for crystallin αB P-Ser-59 (green) was intense in the GCL/NFL compared with control (E-H). In OIR P17 retinas, higher-magnification images of double-immunolabeling of crystallin αB P-Ser-59 with BS-1 lectin (red) showed positive but weaker immunoreactivity of neovascular tufts versus the GCL/NFL (I- L). By western blot, retinal expression of crystallin αB and crystallin αB P-Ser-59 was significantly up-regulated in P12 and P17, compared with that of the control retinas (M, N). In OIR P17 retinas, the expression of crystallin αB P-Ser-59 was more up-regulated, compared with OIR P12 retinas (N). Data are the means ± S.E.M. of the three independent western blot-based measurements. Scale bar: A-H, 20 ㎛; I-L, 10 ㎛. Blue, DAPI.

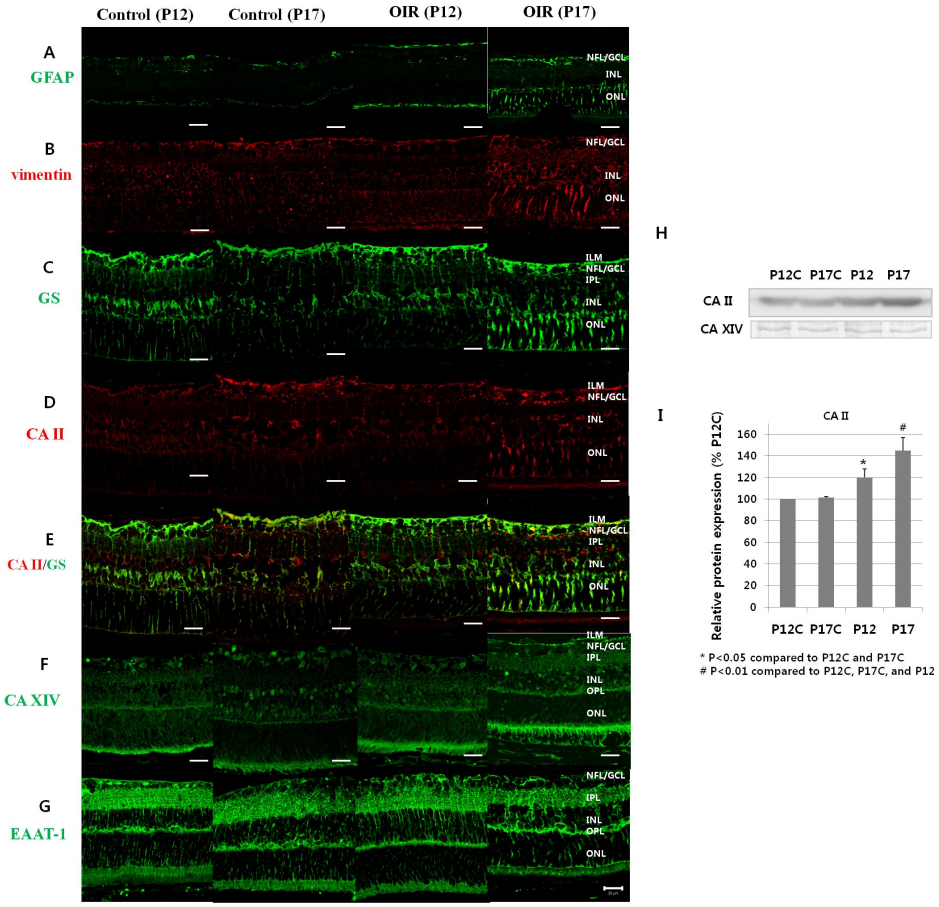

Figure 5. Immunolocalization of proteins expressed primarily in Müller cells.

In oxygen-induced retinopathy (OIR) postnatal Day 17 (P17) retinas, the immunoreactivity for glial fibrillary acidic protein (GFAP), vimentin, and glutamine synthetase (GS) was increased compared with the control and OIR P12 retinas, especially in the distal branches of the Müller cells (A-C). The retinal expression of carbonic anhydrase II (CA II), which was colocalized with GS, increased in OIR P17 retinas (D, E). Quantitation of CA II by western blot showed that CA II was significantly up-regulated in the OIR P12 retina than in the control retinas (H, I). Also, CA II in the OIR P17

retina was more up-regulated than in the OIR P12 and normal control retinas (H, I). Data are the means ± S.E.M. of the three independent western blot-based measurements (I). In contrast, the immunoreactivity for CA XIV in the Müller cells was not changed (F), and the western blot for CA XIV showed no difference between the OIR and control (H). Positive immunoreactivity for excitatory amino acid transporter 1 (EAAT-1) was observed in all retinal layers, without apparent differences between OIR and control retinas (G). P12C and P17C, control eyes enucleated on P12 and P17, respectively. Scale bar: 20 ㎛. NFL/GCL, nerve fiber layer/ ganglion cell layer; INL, inner nuclear layer; ONL, outer nuclear layer.

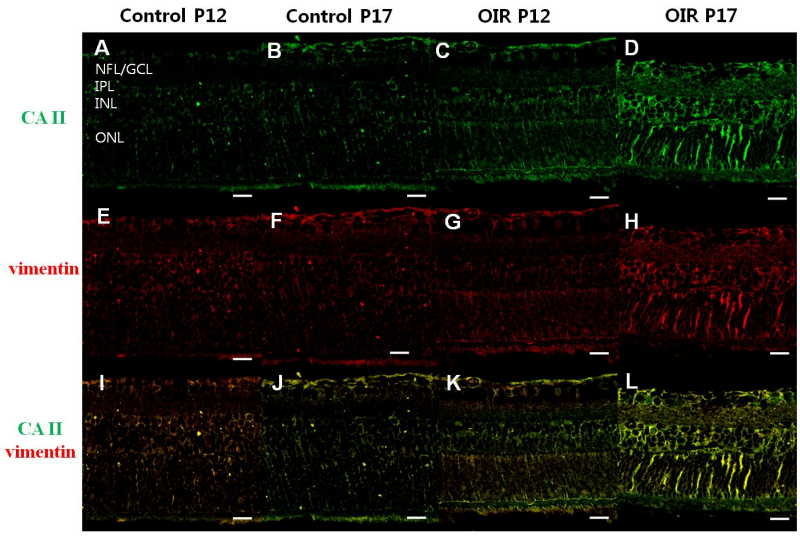

Figure 6. Immunolocalization of carbonic anhydrase II (CA II) and vimentin in oxygen-induced retinopathy (OIR)

In OIR P17 retinas, immunoreactivity for CA II and vimentin was increased compared with controls and OIR P12 retinas, especially in the distal branches of the Müller cells (A-H). Retinal expression of CA II colocalized with vimentin (I-L). NFL, nerve fiber layer; GCL, ganglion cell layer; IPL, inner plexiform layer; INL, inner nuclear layer; ONL, outer nuclear layer. Scale bar, 20 ㎛.

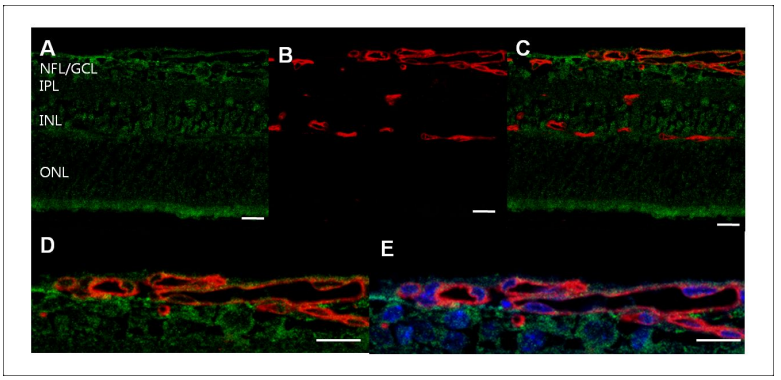

Figure 7. Immunolocalization of phosphoglycerate kinase 1 (PGK1) in oxygen-induced retinopathy (OIR)

In OIR P17 retinas, the immunoreactivity for PGK1 (green) was positive in all retinal layers (A-C) and colocalized weakly with the neovascular tufts (D, E). Blood vessels were stained with TRITC-labeled BS-1 lectin (red), and nuclei were counterstained with DAPI (blue). NFL, nerve fiber layer; GCL, ganglion cell layer; IPL, inner plexiform layer; INL, inner nuclear layer; ONL, outer nuclear layer. Scale bar, 20 ㎛.

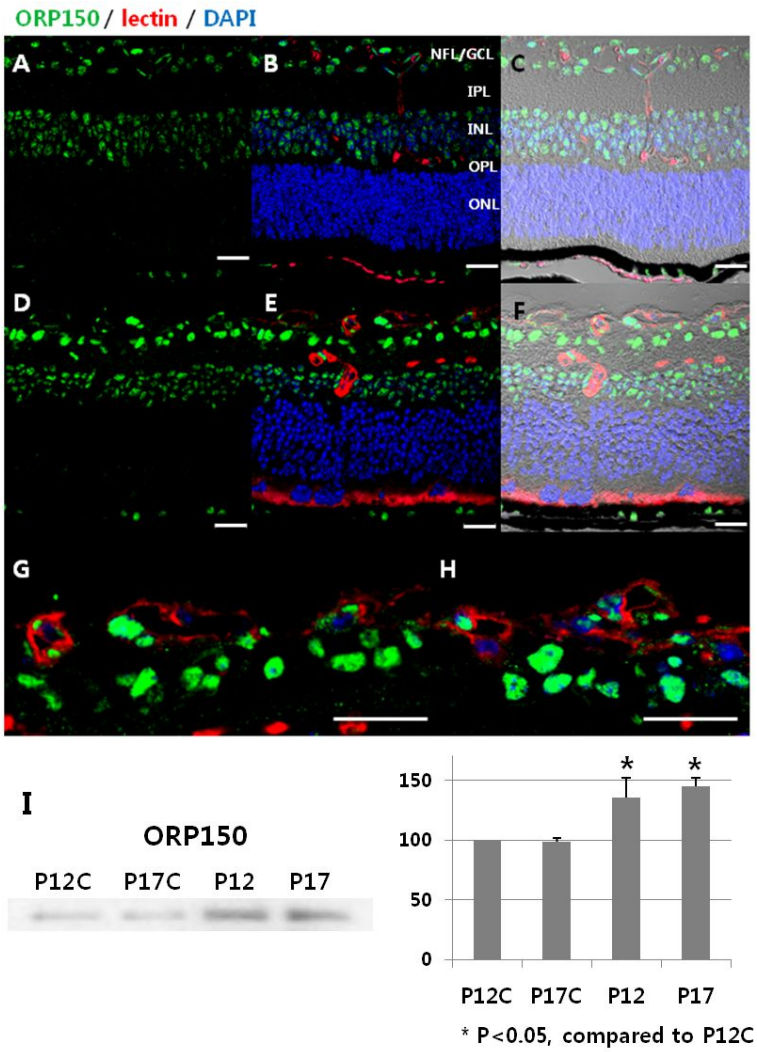

Figure 8. Immunolocalization of 150-kDa oxygen-regulated protein 150 (ORP150) in oxygen-induced retinopathy (OIR).

In the retinal section, immunoreactivity for ORP150 (green) was detected in the perinuclear region of the ganglion cell layer, the inner nuclear layer, and the retinal pigment epithelium layer in control (A, B, C) and OIR postnatal Day 17 (P17) retinas (D, E, F). In OIR P17 retinas, ORP150 colocalized with the neovascular tufts but not with the intraretinal vasculature (G, H). Quantitation of ORP150 by

western blot showed that ORP150 was significantly up-regulated in OIR P12 and P17 retinas, compared with that of the control retinas at P12 and P17 (I). Data are the means ± S.E.M. of the three independent western blot-based measurements. NFL/GCL, nerve fiber layer/ganglion cell layer; IPL, inner plexiform layer; INL, inner nuclear layer; OPL, outer plexiform layer; ONL, outer nuclear layer. Scale bar: 20 ㎛.

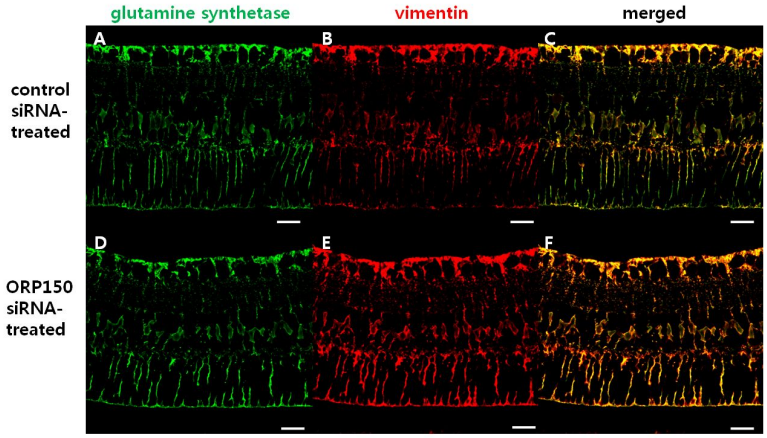

Figure 9. Immunolocalization of 150-kDa oxygen-regulated protein (ORP150) and Iba-1 in oxygen-induced retinopathy (OIR)

In the retinal section, immunoreactivity for ORP150 was not colocalized with immunoreactivity of Iba-1, a microglical marker, in OIR postnatal Day 17 retinas. Scale bar, 20 ㎛.

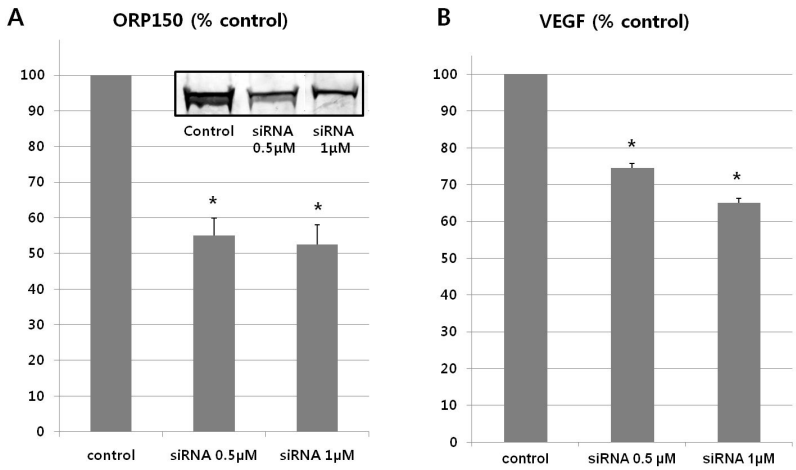

Figure 10. Effect of 150-kDa oxygen-regulated protein (ORP150) knockdown by siRNA on vascular endothelial growth factor (VEGF) secretions in retinal pigment epithelium.

Analysis of protein knockdown in ARPE-19 cells 24 hours after transfection with ORP150 siRNA (A). The graph was generated from densitometric scans of gel bands of a western blot. Additionally, ARPE-19 cell-secreted VEGF was measured by ELISA and decreased significantly 24 hours after transfection (B). Data are the means ± S.E.M. of the three independent experiments. *P < 0.01 vs. control. The value of the control was set to 100%.

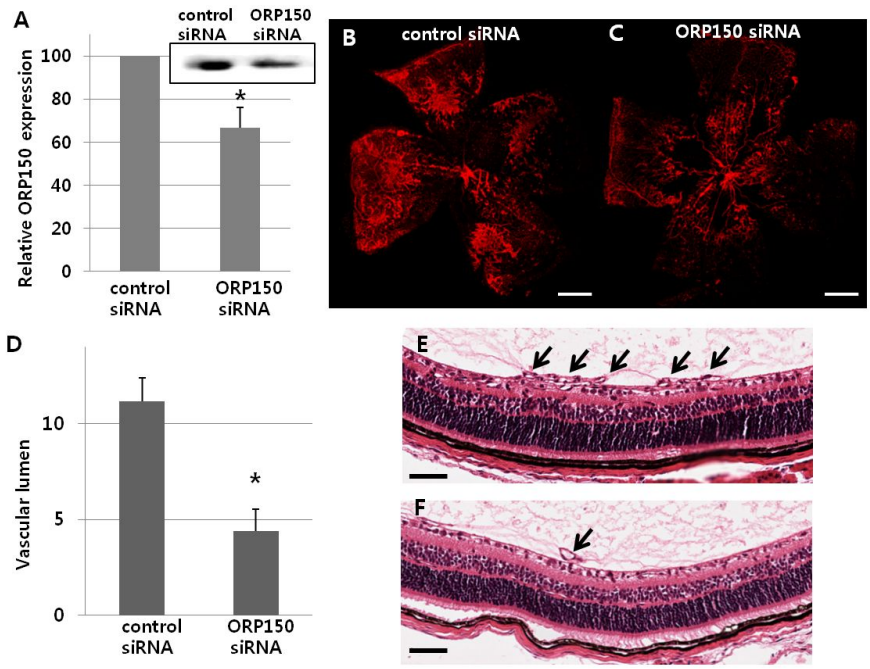

Figure 11. The effect of siRNA targeting 150-kDa oxygen-regulated protein (ORP150) on retinal neovascularization in OIR

Quantitation of ORP150 by western blot showed that intravitreally administered siRNA targeting ORP150 significantly down-regulated retinal expression of ORP150 (A). Data are the means ± S.E.M. of three independent western blot-based measurements. Compared to the control siRNA-treated retina (B), less retinal neovascularization on retinal flat mounts was observed in siRNA targeting ORP150 treated retina (C). Quantitative assessment of retinal neovascularization was done by counting the vascular lumens (arrows) on the vitreal side of the inner limiting membrane (D, E, F). The average lumens per section for each group (n=6 eyes each) are presented as the means ± S.E.M. Note that there is a significant difference in the retinal neovascularization between the control and ORP150 siRNA treated eyes (*$P<0.05$). Scale bar: 500 ㎛ (B,C), 50 ㎛ (E,F).

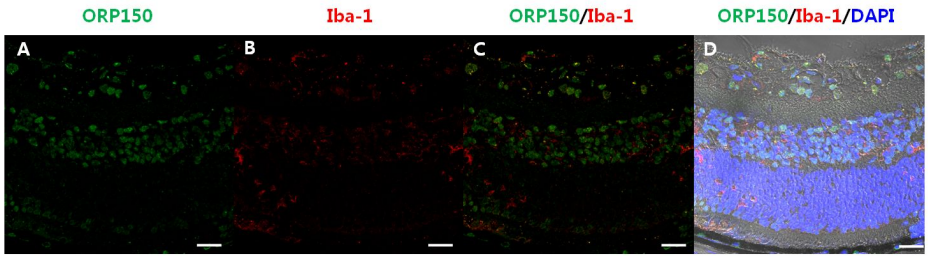

Figure 12. Immunolocalization of glutamine synthetase and vimentin after intravitreal injection of siRNA targeting 150-kDa oxygen-regulated protein (ORP150)

The immunoreactivity for vimentin and glutamine synthetase was not different between control siRNA-treated retina (A-C) and ORP150 siRNA-treated retina (D-F) in a mouse model of oxygen-induced retinopathy. Scale bar, 20 ㎛.

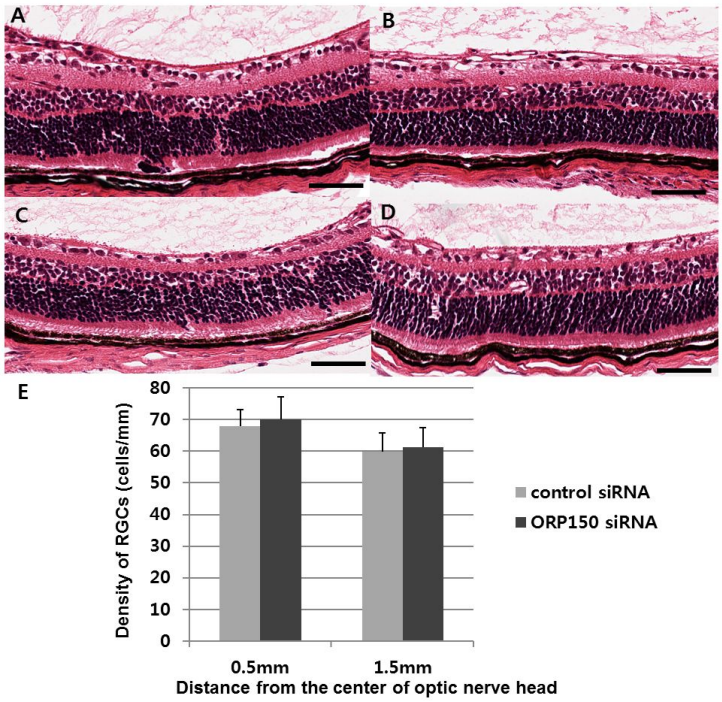

Figure 13. Density of retinal ganglion cells (RGCs) in oxygen-induced retinopathy after intravitreal injection of siRNA targeting 150-kDa oxygen-regulated protein (ORP150)

In hematoxylin and eosin stained retinal sections, densities of RGCs (cells/mm) at 0.5 and 1.5 mm from the center of the optic nerve head were determined in ORP150 siRNA (A, B) and control siRNA injected eyes (C, D). Densities of RGCs (E) showed no statistically significant difference between the two groups ($P>0.05$). Scale bar, 50 ㎛.

Discussion

In this study, the nano-LC-ESI-MS/MS and iTRAQ experiment generated 1422 retinal proteins in the mouse model of OIR and in normally developing mice. Of the differentially expressed proteins between control and OIR retinas, we identified several targets for further study with regard to their function in angiogenesis, vascular change, and neuronal dysfunction in ischemic retinopathy. A comprehensive proteome profile of the developing mouse retina was also acquired in this study. Moreover, proteins of interest, including the crystallin family, CA II and CA XIV, EAAT-1, LEDGF, PGK1, and ORP150, were characterized.

We observed that crystallin proteins, including crystallin αA, αB, βA2, βB2, and βS, were upregulated in OIR retinas. Previous reports have demonstrated upregulation of crystallin αB in OIR,[35] but our findings of upregulation of other crystallin family members in OIR are novel.

Retinal expression of crystallin αA and αB, which belong to the small heat shock protein family, increases by light damage, retinal trauma, and diabetes and declines with optic nerve injuries.[36-38] The overexpression of crystallinαA and αB has neuroprotective effects on retinal ganglion cells.[39] In our study, the increased expression of crystallinαA and αB in ganglion cell layers might also constitute a neuroprotective mechanism in OIR. Kase et al.[35] demonstrated that crystallinαB functions as a chaperone for VEGF-A during retinal angiogenesis. In ourstudy, crystallin αB P-Ser-59 immunoreactivity was robust in the GCL/NFL in P12 and P17 retinas, consistent with Kase et al.[35] However, the immunoreactivity was less intense in the neovascular tufts than in the GCL/NFL in P17, suggesting that the activity of crystallinαB as a chaperone for VEGF-A is more prominent in the inner retinal tissue than in neovascular tufts.

Retinal expression of crystallin βA2 and βB2 increases in animal

models of diabetes and ocular hypertension-induced ganglion cell death.[18,40] In addition, crystallinβB2, expressed primarily in retinal ganglion cells, promotes axonal regeneration.[41] In the OIR model, neuronal dysfunction of the rod and cone, with altered macro- and microglial activity, occurs.[12] Increased beta-crystallin levels might be a neuroprotective mechanism. CrystallinβS, also known as crystallin γS, was upregulated in the outer retinal layer in OIR. Similar to α-crystallins, crystallin βS might be a stress-induced protein, a subfamily of heat-shock proteins with low molecular weights.[42] Despite their implication in several retinal diseases, the function of crystallin family members, other than crystallin αB in OIR, is unknown.

In our study, we identified proteins that were expressed primarily in Müller cells, including glutamine synthetase, GFAP, vimentin, CA II, and EAAT-1. Glutamine synthetase, a marker for specific Müller cell gliosis, in addition to GFAP and vimentin, markers for nonspecific gliosis, was upregulated, especially in the distal branches of Müller cells.[43,44] Reactive gliosis of Müller cells, in response to nearly any pathological change in the retina, has cytoprotective and cytotoxic effects on the retina.[43,44] That several markers of gliosis were upregulated in OIR highlights the significance of Müller cell gliosis during the development of ischemic retinopathy.

In addition, the expression of CA II and XIV, 2 isoforms of CA in the neural retina, has been examined.[45] In the retina, CA has a significant function in pH regulation, fluid absorption, and retinal vascular permeability.[34] In our study, the retinal expression of CA II, a cytoplasmic protein, increased in OIR and colocalized with vimentin and glutamine synthetase. In contrast, immunoreactivity for CA XIV, a membrane-bound protein that is expressed primarily in Müller cells in addition to in RPE, was unchanged in OIR.[46] CAII is elevated in the vitreous of eyes with diabetic retinopathy and raises retinal

vascular permeability[20]—ie, CAII is selectively upregulated in Müller cell gliosis and might contribute to increased retinal vascular permeability in OIR, implicating CA II as a therapeutic target for retinal edema.

In OIR, the molecular mechanisms of neuronal dysfunction are unknown. We observed altered expression of proteins that might be related to this mechanism. EAAT-1, also known as GLAST, the major glutamate transporter of Müller cells, was downregulated in OIR P12 and P17 retinas.[43] Glutamate is transported into Müller cells by glutamate transporters and is converted into the nontoxic amino acid glutamine by glutamine synthetase.[43] Elevated extracellular glutamate is toxic to retinal neurons, suggesting that decreased EAAT-1 levels mediate glutamate toxicity in OIR. In addition, EAAT-1 is required in retinal signal transmission between photoreceptors and bipolar cells and has neuroprotective function during ischemia.[47] Thus, the downregulation of EAAT-1 is a possible mechanism of neuronal dysfunction in OIR.

Acyl-CoA-binding protein (ACBP), also known as diazepam-binding inhibitor, was upregulated in OIR P12 and P17 retinas. In the retina, ACBP is expressed and secreted by Müller cells and might regulate GABAergic activity, which is important for proper function of direction-selective retinal circuitry.[48,49] The effect of increased ACBP levels on GABAergic transmission might be related to neuronal dysfunction in OIR.

Microtubule-associated protein 1 B (MAP1B) was downregulated in OIR P12 retinas but upregulated in OIR P17 retinas. MAP1B, a cytoskeletal element that is highly expressed in the developing nervous system, is believed to modulate the synaptic response in retinal neurons by interacting with specific subunits of retinal GABAc receptors.[50] Because MAP1B deficiency impairs neuronal activity, as demonstrated by decreased amplitude on electroretinograms, changes

in MAP1B in OIR might also be related to neuronal dysfunction in OIR.[51]

Further, LEDGF, a survival factor of the hepatoma-derived growth factor protein family, was also downregulated in OIR P17 retinas compared with OIR P12 retinas. LEDGF, a secreted protein that is induced by stress signals, localizes to the nucleus and activates stress-related genes.[52] Increased endogenous LEDGF and exogenous administration of LEDGF enhance the survival of retinal neurons.[52,53] Thus, the downregulation of LEDGF might also accelerate neuronal dysfunction in OIR. The precise functions of EAAT-1, ACBP, MAP1B, and LEDGF in OIR are unknown, requiring further study.

Angiogenesis-related proteins, such as ORP150 and phosphoglycerate kinase (PGK1), were also upregulated in OIR in our study. ORP150, also known as hypoxia-upregulated protein 1 or glucose-regulated protein 170, is a 999-amino-acid protein that localizes to the endoplasmic reticulum (ER) and is a member of the heat shock protein 70 family.[54] In glioma cell lines, the inhibition of ORP150 expression decreases the release of VEGF, and in ORP150 antisense transfectants, VEGF accumulates in the ER, suggesting a critical function of the inducible ER chaperone ORP150 in tumor-mediated angiogenesis.[55] In our study, the retinal expression of ORP150 increased in OIR and colocalized to the neovascular tufts, implicating ORP150 in pathological retinal angiogenesis. Further, the knockdown of ORP150 by siRNA decreased the level of secreted VEGF in RPE cells, a major source of VEGF in the retina. Moreover, intravitreal administration of siRNA against ORP150 significantly reduced retinal neovascularization in OIR. Thus, the suppression of ORP150 appears to be a therapeutic goal for ameliorating neovascularization in ischemic retinopathy.

In retina, VEGF can be expressed by several cell types, including Müller cells, RPEs, vascular endothelial cells, ganglion cells, glial cells

like astrocytes, and photoreceptors.[56] In OIR, VEGF is highly expressed in the neovascular tufts and the retinal GCL.[57] Also, VEGF receptor-2, one of the two VEGF receptor tyrosine kinases constitutively expressed in the inner nuclear layer and blood vessels in the GCL, is highly expressed in reforming retinal vessels and neovascular tufts in OIR.[56,58] In retinal and choroidal pathological neovascularization, Müller cell- and RPE-derived VEGF are known to be crucial, respectively.[59,60] In our study, ORP150 was expressed in the GCL, INL, RPE layer, and in the neovascular tufts. Müller cells span the entire thickness of the neural retina and the cell bodies lie in the INL. Reduced neovascularization by knock-down of ORP150 by siRNA in OIR might be explained by reduced VEGF secretion mainly from Müller glial cells. Also, VEGF from other glial cells such as astrocytes, and ganglion cells might also be suppressed by knock-down of ORP150.

In addition, ORP150 has cytoprotective effects against ischemia/reperfusion injuries and neuroprotective effects against glutamate toxicity, which might be involved in the neurodegenerative mechanism in OIR, as shown in our study.[61,62] InOIR, ORP150, which is expressed in the retinal GCL and INL, might also effect the stress response for neuronal survival. However, degeneration of retinal ganglion cell was not influenced by knock-down of ORP150.

PGK1, an ATP-generating glycolytic enzyme, is regulated by hypoxia-inducible factor-1α, which also controls VEGF.[63] In prostate cancer cells, the overexpression of PGK1 lowers the secretion of VEGF and increases the generation of angiostatin, which inhibits angiogenesis.[64] The upregulation and expression in neovascular tufts of PGK1 in OIR might regulate retinal angiogenesis. However, its function in OIR is unknown.

In addition to the proteomic changes in OIR, our study generated comprehensive proteome profiles of developing mouse retinas from

P12 and P17. The retinal vasculature remains immature until the end of the third postnatal week, and the neuronal system continues to develop during the first several weeks of life.[65,66] Thus, proteome profiles with quantitation data contribute to research on retinal development.

Previous proteomic studies of retinal pathology revealed many differentially regulated proteins in animal models of diabetic retinopathy, optic nerve injury, and glaucoma.[17,18,67-71] Many proteins such as crystallin family were commonly identified in these studies. Similar to the results of our study, crystallin αA, αB, β, and γ were upregulated in diabetic retina.[18] On the contrary, in the optic nerve injury model, retinal crystallin αA, βS, and βB2 were downregulated.[68] ACBP, which was upregulated in OIR, was also upregulated in diabetic retina and experimental glaucoma/ocular hypertension.[67,70] EAAT-1,which was downregulated in OIR, was upregulated in diabetic retina and the optic nerve injury model.[67,68] MAP1B, which was downregulated in OIR P12 retinas but upregulated in OIR P17 retinas, showed downregulation in the optic nerve injury model and no significant change in diabetic retina.[67,69] The expression patterns of proteins in various retinal disease models may be helpful in understanding the functions of the proteins.

Because the retina is a multi-layered, complex tissue that comprises at least 60 cell types, determining the immunohistochemical localization of differentially regulated proteins is essential for investigating their functions.[71] In our study, the upregulation of crystallin proteins, vimentin, PGK1, and ORP150 has been demonstrated in immunohistochemical staining, but the downregulation of EAAT-1 and LEDGF by iTRAQ was not observed by immunohistochemistry. EAAT-1 and LEDGF are abundant proteins in Müller cells and retinal nuclear layers, respectively. Thus, despite the decreased expression of these proteins, they stained robustly, which

precluded any comparison of the intensities.

Additional studies to determine the function of our proteins of interest are warranted. An examination of the effects of CA II inhibition on retinal vascular permeability, up- or downregulation of PGK1 on the secretion of VEGF and angiostatin in retinal cells, administration of LEDGF in OIR models, and posttranslational modification of crystallin proteins might facilitate identification of new potential therapeutic targets.

In conclusion, using a proteomics discovery method, coupled to targeted approaches, we identified many proteins that were differentially regulated in the mouse model of OIR, some of which might be involved in angiogenesis, vascular change, and neurodegeneration. Examining the differential regulation of the retinal proteome might increase our understanding of the pathophysiology of OIR. Specifically, ORP150 might be a new therapeutic target against retinal angiogenesis in ischemic proliferative retinopathy.

References

1. Sapieha, P.; Joyal, J.S.; Rivera, J.C.; Kermorvant-Duchemin, E.; Sennlaub, F.; Hardy, P.; Lachapelle, P.; Chemtob, S.;Retinopathy of prematurity: understanding ischemic retinal vasculopathies at an extreme of life. J Clin Invest. 2010, 120, 3022-3032.

2. Cheung, N.; Mitchell, P.; Wong, T.Y. Diabetic retinopathy. Lancet. 2010, 376, 124-136.

3. Wong, T.Y.; Scott, I.U. Clinical practice. Retinal-vein occlusion. N Engl J Med. 2010, 363, 2135-2144.

4. Smith, L.E.; Shen, W.; Perruzzi, C.; Soker, S.; Kinose, F.; Xu, X.; Robinson, G.; Driver, S.; Bischoff, J.; Zhang, B.; Schaeffer, J.M.; Senger, D.R. Regulation of vascular endothelial growth factor-dependent retinal neovascularization by insulin-like growth factor-1 receptor. Nat Med. 1999, 5, 1390-1395.

5. Smith, L.E.; Kopchick, J.J.; Chen, W.; Knapp, J.; Kinose, F.; Daley, D.; Foley, E.; Smith, R.G.; Schaeffer, J.M. Essential role of growth hormone in ischemia-induced retinal neovascularization. Science. 1997, 276, 1706-1709.

6. Chen, J.; Connor, K.M.; Aderman, C.M.; Smith, L.E. Erythropoietin deficiency decreases vascular stability in mice. J Clin Invest. 2008, 118, 526-533.

7. Drixler, T.A.; BorelRinkes, I.H.; Ritchie, E.D.; Treffers, F.W.; van Vroonhoven, T.J.; Gebbink, M.F.; Voest, E.E. Angiostatin inhibits pathological but not physiological retinal angiogenesis. Invest Ophthalmol Vis Sci. 2001, 42, 3325-3330.

8. Stellmach, V.; Crawford, S.E.; Zhou, W.; Bouck, N. Prevention of ischemia-induced retinopathy by the natural ocular antiangiogenic agent pigment epithelium-derived factor. Proc Natl Acad Sci U S A. 2001, 27, 2593-2597.

9. Kojima, H.; Otani, A.; Oishi, A.; Makiyama, Y.; Nakagawa, S.; Yoshimura, N. Granulocyte colony-stimulating factor attenuates oxidative stress-induced apoptosis in vascular endothelial cells and exhibits functional and morphologic protective effect in oxygen-inducedretinopathy. Blood. 2011, 117, 1091-1100.

10. Tang, Y.; Scheef, E.A.; Wang, S.; Sorenson, C.M.; Marcus, C.B.;

Jefcoate, C.R.; Sheibani, N. CYP1B1 expression promotes the proangiogenic phenotype of endothelium through decreased intracellular oxidative stress and thrombospondin-2 expression. Blood. 2009, 113, 744-754.
11. Kermorvant-Duchemin, E.; Sapieha, P.; Sirinyan, M.; Beauchamp, M.; Checchin, D.; Hardy, P.; Sennlaub, F.; Lachapelle, P.; Chemtob, S. Understanding ischemic retinopathies: emerging concepts from oxygen-induced retinopathy. Doc Ophthalmol. 2010, 120, 51-60.
12. Vessey, K.A.; Wilkinson-Berka, J.L.; Fletcher, E.L. Characterization of retinal function and glial cell response in a mouse model of oxygen-induced retinopathy. J Comp Neurol. 2011, 519, 506-527.
13. Tannu, N.S.; Hemby, S.E. Methods for proteomics in neuroscience. Prog Brain Res. 2006, 158, 41-82.
14. Kim, S.J.; Kim, S.; Park, J.; Lee, H.K.; Park, K.S.;Yu, H.G.;Kim, Y. Differential expression of vitreous proteins in proliferative diabetic retinopathy. Curr Eye Res. 2006, 31, 231-240.
15. Kim, T.; Kim, S.J.; Kim, K.; Kang, U.B.; Lee, C.; Park, K.S.; Yu, H.G.; Kim, Y. Profiling of vitreous proteomes from proliferative diabetic retinopathy and nondiabetic patients. Proteomics. 2007, 7, 4203-4215.
16. Kim, K.; Kim, S.J.; Yu, H.G.; Yu, J; Park, K.S.; Jang, I.J.; Kim, Y. Verification of biomarkers for diabetic retinopathy by multiple reaction monitoring. J Proteome Res. 2010, 9, 689-699.
17. Gao, B.B.; Phipps, J.A.; Bursell, D.; Clermont, A.C.; Feener, E.P. Angiotensin AT1 receptor antagonism ameliorates murine retinal proteome changes induced by diabetes.J Proteome Res. 2009, 8, 5541-5549.
18. Fort, P.E.; Freeman, W.M.; Losiewicz, M.K.; Singh, R.S.; Gardner, T.W. The retinal proteome in experimental diabetic retinopathy: up-regulation of crystallins and reversal by systemic and periocular insulin. Mol Cell Proteomics. 2009, 8, 767-779.
19. Gao, B.B.; Chen, X.; Timothy, N.; Aiello, L.P.; Feener, E.P. Characterization of the vitreous proteome in diabetes without diabetic retinopathy and diabetes with proliferative diabetic retinopathy. J Proteome Res. 2008, 7, 2516-2525.
20. Gao, B.B.; Clermont, A.; Rook, S.; Fonda, S.J.; Srinivasan, V.J.; Wojtkowski, M.; Fujimoto, J.G.; Avery, R.L.; Arrigg, P.G.; Bursell, S.E.;

Aiello, L.P.; Feener, E.P. Extracellular carbonic anhydrase mediates hemorrhagic retinal and cerebral vascular permeability through prekallikrein activation. Nat Med. 2007, 13, 181-188.
21. Smith, L.E.; Wesolowski, E.; McLellan, A.; Kostyk, S.K.; D'Amato, R.; Sullivan, R.; D'Amore, P.A. Oxygen-inducedretinopathy in the mouse. Invest Ophthalmol Vis Sci. 1994, 35, 101-111.
22. Penn, J.S.; Tolman, B.L.; Lowery, L.A. Variable oxygen exposure causes preretinal neovascularization in the newborn rat. Invest Ophthalmol Vis Sci. 1993, 34, 576-585.
23. Connor, K.M.; Krah, N.M.; Dennison, R.J.; Aderman, C.M.; Chen, J.; Guerin, K.I.; Sapieha, P.; Stahl, A.; Willett, K.L.; Smith, L.E. Quantification of oxygen-induced retinopathy in the mouse: a model of vessel loss, vessel regrowth and pathological angiogenesis. Nat Protoc. 2009, 4, 1565-1573.
24. Grossniklaus, H.E.; Kang, S.J.; Berglin, L. Animal models of choroidal and retinal neovascularization. Prog Retin Eye Res. 2010, 29, 500-519.
25. Jin, J.; Kwon, Y. W.; Paek, J. S.; Cho, H. J.; Yu, J.; Lee, J. Y.; Chu, I. S.; Park, I. H.; Park, Y. B.; Kim, H. S.; Kim, Y., Analysis of differential proteomes of induced pluripotent stem cells by protein-based reprogramming of fibroblasts. J Proteome Res. 2011, 10, 977-989.
26. Jin, J.; Park, J.; Kim, K.; Kang, Y.; Park, S. G.; Kim, J. H.; Park, K. S.; Jun, H.; Kim, Y., Detection of differential proteomes of human beta-cells during islet-like differentiation using iTRAQ labeling. J Proteome Res. 2009, 8, 1393-1403.
27. Keller, A.; Nesvizhskii, A. I.; Kolker, E.; Aebersold, R. Empirical statistical model to estimate the accuracy of peptide identifications made by MS/MS and database search. Anal Chem 2002, 74, 5383-5392.
28. Nesvizhskii, A. I.; Keller, A.; Kolker, E.; Aebersold, R. A statistical model for identifying proteins by tandem mass spectrometry. Anal Chem. 2003, 75, 4646-4658.
29. Lim, Y.; Jo, D.H.; Kim, J.H.; Ahn, J.H.; Hwang, Y.K.; Kang, D.K.; Chang, S.I.; Yu, Y.S.; Yoon, Y.; Kim, J.H. Human apolipoprotein(a) kringle V inhibits ischemia-induced retinal neovascularization via suppression of fibronectin-mediated angiogenesis. Diabetes. 2012, 61,1599-1608.
30. Goto, W.; Ota, T.; Morikawa, N.; Otori, Y.; Hara, H.; Kawazu, K.;

Miyawaki, N.; Tano, Y. Protective effects of timolol against the neuronal damage induced by glutamate and ischemia in the rat retina. Brain Res. 2002, 958, 10-19.
31. Seki, M.; Tanaka, T.; Matsuda, H.; Togano, T.; Hashimoto, K.; Ueda, J.; Fukuchi, T.; Abe, H. Topically administered timolol and dorzolamide reduce intraocular pressure and protect retinal ganglion cells in a rat experimental glaucoma model. Br J Ophthalmol. 2005, 89, 504-507.
32. Han, C. L.; Chen, J. S.; Chan, E. C.; Wu, C. P.; Yu, K. H.; Chen, K. T.; Tsou, C. C.; Tsai, C. F.; Chien, C. W.; Kuo, Y. B.; Lin, P. Y.; Yu, J. S.; Hsueh, C.; Chen, M. C.; Chan, C. C.; Chang, Y. S.; Chen, Y. J. An informatics-assisted label-free approach for personalized tissue membrane proteomics: case study on colorectal cancer. Mol Cell Proteomics. 2011, 10.M110.003087.
33. Ecroyd, H.; Meehan, S.; Horwitz, J.; Aquilina, J.A.; Benesch, J.L.; Robinson, C.V.; Macphee, C.E.; Carver, J.A. Mimicking phosphorylation of alphaB-crystallin affects its chaperone activity. Biochem J. 2007, 401, 129-141.
34. Weiwei, Z.; Hu, R. Targetingc arbonic anhydrase to treatdiabetic retinopathy: emerging evidences and encouraging results. Biochem Biophys Res Commun. 2009, 390, 368-371.
35. Kase, S.; He, S.; Sonoda, S.; Kitamura, M.; Spee, C.; Wawrousek, E.; Ryan, S.J.; Kannan, R.; Hinton, D.R. alphaB-crystallin regulation of angiogenesis by modulation of VEGF. Blood. 2010, 115, 3398-3406.
36. Fort, P.E.; Lampi, K.J. New focus on alpha-crystallins in retinal neurodegenerative diseases.Exp Eye Res. 2011, 92, 98-103.
37. Sakaguchi, H.; Miyagi, M.; Darrow, R.M.; Crabb, J.S.; Hollyfield, J.G.; Organisciak, D.T.; Crabb, J.W. Intense light exposure changes the crystallin content in retina. Exp Eye Res. 2003, 76, 131-133.
38. Vázquez-Chona, F.; Song, B.K.; Geisert, E.E. Jr. Temporal changes in gene expression after injury in the rat retina. Invest Ophthalmol Vis Sci. 2004, 45, 2737-2746.
39. Munemasa, Y.; Kwong, J.M.; Caprioli, J.; Piri, N. The role of alphaA- and alphaB-crystallins in the survival of retinal ganglion cells after optic nerve axotomy. Invest Ophthalmol Vis Sci. 2009, 50, 3869-3875.

40. Piri, N.; Song, M.; Kwong, J.M.; Caprioli, J. Modulation of alpha and beta crystallin expression in rat retinas with ocular hypertension-induced ganglion cell degeneration. Brain Res. 2007, 1141, 1-9.
41. Liedtke, T.; Schwamborn, J.C.; Schröer, U.; Thanos, S. Elongation of axons during regeneration involves retinal crystallin beta b2 (crybb2).Mol Cell Proteomics. 2007, 6, 895-907.
42. Sinha, D.; Esumi, N.; Jaworski, C.; Kozak, C.A.; Pierce, E.; Wistow, G. Cloning and mapping the mouse Crygs gene and non-lens expression of [gamma]S-crystallin. Mol Vis. 1998, 4, 8.
43. Bringmann, A.; Pannicke, T.; Grosche, J.; Francke, M.; Wiedemann, P.; Skatchkov, S.N.; Osborne, N.N.; Reichenbach, A. Müller cells in the healthy and diseased retina. Prog Retin Eye Res. 2006, 25, 397-424.
44. Bringmann, A.; Iandiev, I.; Pannicke, T.; Wurm, A.; Hollborn, M.; Wiedemann, P.; Osborne, N.N.; Reichenbach, A. Cellular signaling and factorsinvolved in Müller cellgliosis: neuroprotective and detrimental effects. Prog Retin Eye Res. 2009, 28, 423-451.
45. Nagelhus, E.A.; Mathiisen, T.M.; Bateman, A.C.; Haug, F.M.; Ottersen, O.P.; Grubb, J.H.; Waheed, A.; Sly, W.S. Carbonic anhydrase XIV is enriched in specific membrane domains of retinal pigment epithelium, Muller cells, and astrocytes. Proc Natl Acad Sci U S A. 2005, 102, 8030-8035.
46. Weiwei, Z.; Hu, R. Targeting carbonic anhydrase to treat diabetic retinopathy: emerging evidences and encouraging results.BiochemBiophys Res Commun. 2009, 390, 368-371.
47. Harada, T.; Harada, C.; Watanabe, M.; Inoue, Y.; Sakagawa, T.; Nakayama, N.; Sasaki, S.; Okuyama, S.; Watase, K.; Wada, K.; Tanaka, K. Functions of the two glutamate transporters GLAST and GLT-1 in the retina. Proc Natl Acad Sci U S A. 1998, 95, 4663-4666.
48. Barmack, N.H.; Bilderback, T.R.; Liu, H.; Qian, Z.; Yakhnitsa, V. Activity-dependent expression of acyl-coenzyme a-binding protein in retinal muller glial cells evoked by optokinetic stimulation. J Neurosci. 2004, 24, 1023-1033.
49. Qian, Z.; Bilderback, T.R.; Barmack, N.H.Acyl coenzyme A-bindingprotein (ACBP) is phosphorylated and secreted by retinal Müller astrocytes following protein kinase C activation.J Neurochem. 2008, 105, 1287-1299.

50. Hanley, J.G.; Koulen, P.; Bedford, F.; Gordon-Weeks, P.R.; Moss, S.J. The protein MAP-1B links GABA(C) receptors to the cytoskeleton at retinal synapses. Nature. 1999, 397, 66-69.
51. Pangratz-Fuehrer, S.; Bubna-Littitz, H.; Propst, F.; Reitsamer, H. Mice deficient in microtubule-associated protein MAP1B show a distinct behavioral phenotype and altered retina function. Behav Brain Res. 2005, 164, 188-196.
52. Shinohara, T.; Singh, D.P.; Fatma, N. LEDGF, a survival factor, activates stress-related genes. Prog Retin Eye Res. 2002, 21, 341-358.
53. Raz-Prag, D.; Zeng, Y.; Sieving, P.A.; Bush, R.A. Photoreceptor protection by adeno-associated virus-mediated LEDGF expression in the RCS rat model of retinal degeneration: probing the mechanism. Invest Ophthalmol Vis Sci. 2009, 50, 3897-3906.
54. Kuwabara, K.; Matsumoto, M.; Ikeda, J.; Hori, O.; Ogawa, S.; Maeda, Y.; Kitagawa, K.; Imuta, N.; Kinoshita, T.; Stern, D.M.; Yanagi, H.; Kamada, T. Purification and characterization of a novel stress protein, the 150-kDa oxygen-regulated protein (ORP150), from cultured rat astrocytes and its expression in ischemic mouse brain. J Biol Chem. 1996, 271, 5025-5032.
55. Ozawa, K.; Tsukamoto, Y.; Hori, O.; Kitao, Y.; Yanagi, H.; Stern, D.M.; Ogawa, S. Regulation of tumor angiogenesis by oxygen-regulated protein 150, an inducible endoplasmic reticulum chaperone. Cancer Res. 2001, 61, 4206-4213.
56. Kim, I.; Ryan, A.M.; Rohan, R.; Amano, S.; Agular, S.; Miller, J.W.; Adamis, A.P. Constitutive expression of VEGF, VEGFR-1, and VEGFR-2 in normal eyes. Invest Ophthalmol Vis Sci. 1999, 40, 2115-2121.
57. Zhao, M.; Shi, X.; Liang, J.; Miao, Y.; Xie, W.; Zhang, Y.; Li, X. Expression of pro- and anti-angiogenic isoforms of VEGF in the mouse model of oxygen-induced retinopathy. Exp Eye Res. 2011, 93, 921-926.
58. McLeod, D.S.; Taomoto, M.; Cao, J.; Zhu, Z.; Witte, L.; Lutty, G.A. Localization of VEGF receptor-2 (KDR/Flk-1) and effects of blocking it in oxygen-induced retinopathy. Invest Ophthalmol Vis Sci. 2002, 43, 474-482.
59. Bai, Y.; Ma, J.X.; Guo, J.; Wang, J.; Zhu, M.; Chen, Y.; Le, Y.Z. Müller cell-derived VEGF is a significant contributor to retinal neovascularization. J Pathol. 2009, 219, 446-454.

60. Spilsbury, K.; Garrett, K.L.; Shen, W.Y.; Constable, I.J.; Rakoczy, P.E. Overexpression of vascular endothelial growth factor (VEGF) in the retinal pigment epithelium leads to the development of choroidal neovascularization. Am J Pathol. 2000, 157, 135-144.
61. Kitao, Y.; Ozawa, K.; Miyazaki, M.; Tamatani, M.; Kobayashi, T.; Yanagi, H.; Okabe, M.; Ikawa, M.; Yamashima, T.; Stern, D.M.; Hori, O.; Ogawa, S. Expression of the endoplasmic reticulum molecular chaperone (ORP150) rescues hippocampal neurons from glutamate toxicity. J Clin Invest. 2001, 108, 1439-1450.
62. Kitano, H.; Nishimura, H.; Tachibana, H.; Yoshikawa, H.; Matsuyama, T. ORP150 ameliorates ischemia/reperfusion injury from middle cerebral artery occlusion in mouse brain. Brain Res. 2004, 1015, 122-128.
63. Semenza, G.L.; Roth, P.H.; Fang, H.M.; Wang, G.L. Transcriptional regulation of genes encoding glycolytic enzymes by hypoxia-inducible factor 1.J Biol Chem. 1994, 269, 23757-23763.
64. Wang, J.; Wang, J.; Dai, J.; Jung, Y.; Wei, C.L.; Wang, Y.; Havens, A.M.; Hogg, P.J.; Keller, E.T.; Pienta, K.J.; Nor, J.E.; Wang, C.Y.; Taichman, R.S. A glycolytic mechanism regulating an angiogenic switch in prostate cancer. Cancer Res. 2007, 67, 149-159.
65. Stahl, A.; Connor, K.M.; Sapieha, P.; Chen, J.; Dennison, R.J.; Krah, N.M.; Seaward, M.R.; Willett, K.L.; Aderman, C.M.; Guerin, K.I.; Hua, J.; Löfqvist, C.; Hellström, A.; Smith, L.E. The mouse retina as an angiogenesis model. Invest Ophthalmol Vis Sci. 2010, 51, 2813-2826.
66. Coombs, J.L.;Van Der List, D.;Chalupa, L.M. Morphological properties of mouse retinal ganglion cells during postnatal development. J Comp Neurol. 2007, 503, 803-814.
67. VanGuilder, H.D.; Bixler, G.V.; Kutzler, L.; Brucklacher, R.M.; Bronson, S.K.; Kimball, S.R.; Freeman, W.M. Multi-modal proteomic analysis of retinal protein expression alterations in a rat model of diabetic retinopathy. PLoS One. 2011, 6, e16271.
68. Magharious, M.; D'Onofrio, P.M.; Hollander, A.; Zhu, P.; Chen, J.; Koeberle, P.D. Quantitative iTRAQ analysis of retinal ganglion celldegeneration after optic nerve crush. J Proteome Res. 2011, 10, 3344-3362.
69. Hollander, A.; D'Onofrio, P.M.; Magharious, M.M.; Lysko, M.D.; Koeberle,

P.D. Quantitative retinal protein analysis after optic nerve transection reveals a neuroprotective role for hepatoma-derived growth factor on injured retinal ganglion cells. Invest Ophthalmol Vis Sci. 2012, 53, 3973-3989.
70. Crabb, J.W.; Yuan, X.; Dvoriantchikova, G.; Ivanov, D.; Crabb, J.S.; Shestopalov, V.I. Preliminary quantitative proteomic characterization of glaucomatous rat retinal ganglion cells. Exp Eye Res. 2010, 91, 107-110.
71. Kolb, H.;Nelson, R.; Ahnelt, P.; Cuenca, N. Cellular organization of the vertebrate retina.Prog Brain Res. 2001, 131, 3-26.

국문 초록

실명을 유발하는 허혈성 망막병증의 모델인 산소유발망막병증의 발생 기전과 관련된 새로운 단백질들을 동정하기 위해 산소유발망막병증 마우스의 망막 단백체를 정량적으로 분석하였다. 산소유발망막병증은 C57BL/6 마우스를 생후 7일째부터 5일간 75%의 고농도 산소 환경에, 이후 5일간은 정상 산소 환경에 노출시켜 유발하였다. 생후 12일째 및 17일째 정상 및 산소유발망막병증 마우스의 망막을 isobaric tags for relative and absolute quantitation (iTRAQ)과 nano-LC-ESI-MS/MS로 분석하였다. 총 1422개의 망막 단백질 - iTRAQ 분석으로 699개, nano-LC-ESI-MS/MS 분석으로 1074개-이 동정되었다. iTRAQ 분석에서, 대조군 망막과 비교해 산소유발망막병증에서는 생후 17일째에 21개 및 17개의 단백질이, 생후 12일째에 25개 및 14개의 단백질이 각각 유의하게 증가 또는 감소하였다. 발현이 변화한 단백질 중 crystallin 단백질과 뮐러세포 관련 단백질, 신경 변성 관련 단백질, 그리고 150-kDa oxygen-regulated protein (ORP150) 등 혈관신생 관련 단백질에 대해 추가 분석을 시행하였다. ORP150은 망막 신생혈관과 같은 위치에 발현되었고 ORP150의 발현을 siRNA로 억제한 결과 배양한 망막색소상피세포의 혈관내피성장인자 분비량이 감소하였다. 또한, 산소유발망막병증 모델에서 ORP150의 발현을 억제하는 siRNA를 유리체강내 주사한 결과, 망막의 신생혈관이 감소되었다. 결론적으로, 단백체 분석 및 표적 단백질 분석으로 산소유발망막병증 마우스 모델의 망막에서 발현이 변화한 단백질을 다수 발견하였다. ORP150 등 이들 단백질은 혈관증식성 망막병증의 새로운 치료 표적 단백질의 가능성이 있다.

* 본 내용은 Journal of Proteome Research (Sang Jin Kim, Jonghwa Jin, Young Joo Kim, Youngsoo Kim, Hyeong Gon Yu. Retinal proteome analysis in a mouse model of oxygen-induced retinopathy. J Proteome Res. 2012;11:5186-203.)에 출판 완료된 내용임.

주요어 : 산소유발망막병증, iTRAQ, 혈관신생, crystallin, 150-kDa

oxygen-regulated protein, 뮐러세포.
학번 : 2009-30505